Astronomy & Astrophysics manuscript no. February 1, 2008
(DOI: will be inserted by hand later)

arXiv:astro-ph/0207176v1 8 Jul 2002

Radio Sources in Low-Luminosity Active Galactic Nuclei.

III. "AGNs" in a Distance-Limited Sample of "LLAGNs"

Neil M. Nagar[1], Heino Falcke[2], Andrew S. Wilson[3], and James S. Ulvestad[4]

[1] Arcetri Observatory, Largo E. Fermi 5, Florence 50125, Italy
e-mail: `neil@arcetri.astro.it`
[2] Max-Planck-Institut für Radioastronomie, Auf dem Hügel 69, 53121 Bonn, Germany
e-mail: `hfalcke@mpifr-bonn.mpg.de`
[3] Department of Astronomy, University of Maryland, College Park, MD 20742, U.S.A.
Adjunct Astronomer, Space Telescope Science Institute, 3700 San Martin Drive, Baltimore, MD 21218, U.S.A.
e-mail: `wilson@astro.umd.edu`
[4] National Radio Astronomy Observatory, P.O. Box 0, Socorro, NM 87801, U.S.A.
e-mail: `julvesta@nrao.edu`

Received January 23, 2002; accepted June 7, 2002

Abstract. This paper presents the results of a high resolution radio imaging survey of all known (96) low-luminosity active galactic nuclei (LLAGNs) at $D \leq 19$ Mpc. We first report new 2 cm (150 mas resolution using the VLA) and 6 cm (2 mas resolution using the VLBA) radio observations of the previously unobserved nuclei in our samples and then present results on the complete survey. We find that almost half of all LINERs and low-luminosity Seyferts have flat-spectrum radio cores when observed at 150 mas resolution. Higher (2 mas) resolution observations of a flux-limited subsample have provided a 100% (16 of 16) detection rate of pc-scale radio cores, with implied brightness temperatures $\gtrsim 10^8$ K. The five LLAGNs with the highest core radio fluxes also have pc-scale 'jets.' Compact radio cores are almost exclusively found in massive ellipticals and in type 1 nuclei (i.e. nuclei with broad Hα emission). Only a few 'transition' nuclei have compact radio cores; those detected in the radio have optical emission-line diagnostic ratios close to those of LINERs/Seyferts. This indicates that some transition nuclei are truly composite Seyfert/LINER+H II region nuclei, with the radio core power depending on the strength of the former component. The core radio power is correlated with the nuclear optical 'broad' Hα luminosity, the nuclear optical 'narrow' emission-line luminosity and width, and with the galaxy luminosity. In these correlations LLAGNs fall close to the low-luminosity extrapolations of more powerful AGNs. The scalings suggest that many of the radio-non-detected LLAGNs are simply lower power versions of the radio-detected LLAGNs. The ratio of core radio power to nuclear optical emission-line luminosity increases with increasing bulge luminosity for all LLAGNs. Also, there is evidence that the luminosity of the disk component of the galaxy is correlated with the nuclear emission-line luminosity (but not the core radio power). About half of all LLAGNs with multiple epoch data show significant inter-year radio variability. Investigation of a sample of ~ 150 nearby bright galaxies, most of them LLAGNs, shows that the nuclear ($\leq$150 mas size) radio power is strongly correlated with both the black hole mass and the galaxy bulge luminosity; linear regression fits to all ~ 150 galaxies give: $\log P_{2\mathrm{cm}} = 1.31(\pm 0.16) \log M_{\mathrm{MDO}} + 8.77$ and $\log P_{2\mathrm{cm}} = 1.89(\pm 0.21) \log L_{\mathrm{B}}(\mathrm{bulge}) - 0.17$. Low accretion rates ($\leq 10^{-2} - 10^{-3}$ of the Eddington rate) are implied in both advection- and jet-type models. In brief, all evidence points towards the presence of accreting massive black holes in a large fraction, perhaps all, of LLAGNs, with the nuclear radio emission originating in either the accretion inflow onto the massive black hole or from jets launched by this black hole - accretion disk system.

Key words. accretion, accretion disks — galaxies: active — galaxies: jets — galaxies: nuclei — radio continuum: galaxies — surveys

1. Introduction

The debate on the power source of low-luminosity active galactic nuclei (LLAGNs, i.e. low-luminosity Seyferts, LINERs, and "transition" nuclei [nuclei with spectra intermediate between those of LINERs and H II regions]) is a continuing one. Their low emission-line luminosities ($L_{\mathrm{H}\alpha} \leq 10^{40}$ erg s^{-1} by definition; Ho et al., 1997a, hereafter H97a) can be modeled in terms of photoionization by

---

Send offprint requests to: Neil M. Nagar hot, young stars (Terlevich & Melnick, 1985; Filippenko & Terlevich, 1992; Shields, 1992), by collisional ionization in shocks (Koski & Osterbrock, 1976; Fosbury et al., 1978; Heckman, 1980; Dopita & Sutherland, 1995) or by aging starbursts (Alonso-Herrero et al., 1999).

On the other hand, evidence has been accumulating that at least some fraction of LLAGNs share characteristics in common with their more powerful counterparts - radio galaxies and powerful Seyfert galaxies. These similarities include the presence of compact nuclear radio cores (Heckman, 1980), water vapor megamasers (Braatz et al., 1997), nuclear point-like UV sources (Maoz et al., 1995; Barth et al., 1998), broad Hα lines (Ho et al., 1997c, hereafter H97c), and broader Hα lines in polarized emission than in total emission (Barth et al., 1999). If LLAGNs are truly scaled down AGNs then the challenge is to explain their much lower accretion luminosities. This requires either very low accretion rates ($\sim 10^{-8}$ of the Eddington accretion rate, $L_{\rm Edd}$) or radiative efficiencies (the ratio of radiated energy to accreted mass) much lower than the typical value of $\sim$10% (e.g. Chapter 7.8 of Frank, King, & Raine, 1995) assumed for powerful AGNs.

One well-known property of some powerful AGNs is a compact (sub-parsec), flat-spectrum (usually defined as $\alpha \geq -0.5$, $S_\nu \propto \nu^\alpha$) nuclear radio source, usually interpreted as the synchrotron self-absorbed base of the jet which fuels larger-scale radio emission. Astrophysical jets are known to be produced in systems undergoing accretion onto a compact object (e.g. Pringle, 1993; Blandford, 1993) so such compact radio sources in galactic nuclei may reasonably be considered a signature of an AGN. Much theoretical work (e.g. Begelman, Blandford, & Rees, 1984; Lovelace & Romanova, 1996; Falcke & Biermann, 1999) has been devoted to this disk-jet relationship in the case of galactic nuclei and it has been suggested that scaled-down versions of AGN jets can produce flat-spectrum radio cores in LLAGNs (Falcke & Biermann, 1999). Compact nuclear radio emission with a flat to inverted spectrum is also expected from the accretion inflow in advection-dominated (ADAF; Narayan et al., 1998) or convection-dominated (CDAF; Narayan et al., 2000) accretion flows, possible forms of accretion onto a black hole at low accretion rates (Rees et al., 1982). Flat-spectrum radio sources can also result through thermal emission from ionized gas in normal H II regions or through free-free absorption of non-thermal radio emission, a process which probably occurs in compact nuclear starbursts (Condon et al., 1991). The brightness temperature, $T_{\rm b}$, in such starbursts is limited to log $[T_{\rm b}$ (K)$] \lesssim 5$ (Condon et al., 1991). Thus it is necessary to show that $T_{\rm b}$ exceeds this limit before accretion onto a black hole can be claimed as the power source.

From the observational perspective, Heckman (1980) showed that LINER nuclei tend to be associated with a compact radio source, and compact, flat-spectrum radio cores are known to be present in many 'normal' E/S0 galaxies (Sadler et al., 1989; Wrobel & Heeschen, 1991; Slee et al., 1994). Flat-spectrum radio cores are, however, uncommon in normal spirals or Seyfert galaxies (Ulvestad & Wilson, 1989; Vila et al., 1990; Sadler et al., 1995), though Ulvestad & Ho (2001a) have pointed out that low-luminosity Seyferts have a higher incidence of flat-spectrum cores than more powerful Seyferts.

How does one distinguish accretion-powered LLAGNs from LLAGNs powered by hot stars or supernova shocks? Broad Hα lines and bright unresolved optical or UV sources are ambiguous indicators because they can all be produced in starburst models (see Terlevich et al., 1992). Searches for broader polarized Hα emission are currently feasible in only a few of the brightest LLAGNs (Barth et al., 1999). X-ray emission from the nucleus can be confused with sources in the bulge or disk of the galaxy, even at *Chandra*'s sub arcsecond resolution. Further, all these indicators may be affected by viewing geometry, obscuration, and the signal-to-noise of the observations, the last problem being exacerbated by the low optical, UV, and X-ray luminosities of LLAGNs and the need to subtract the starlight. The radio regime, however, offers several advantages. Gigahertz (cm wave) radiation does not suffer the obscuration that affects the UV to infra-red. Also, at tens of gigahertz the problems of free-free absorption can be avoided in most cases. Finally, high resolution, high sensitivity radio maps can be routinely made with an investment of less than an hour per source at the Very Large Array[1] (VLA; Thompson et al., 1980) and the Very Long Baseline Array (VLBA; Napier et al., 1994). At their resolutions of $\sim$100 milli-arcsec (mas) and $\sim$1 mas, respectively, it is easy to pick out the AGN, since any other radio emission from the galaxy is usually resolved out.

Closely related to these theoretical and observational issues are the increasing number of accurate mass determinations for "massive dark objects" (MDOs) in nearby galactic nuclei. Indeed, dynamic signatures of nuclear black holes are being found in almost every nearby galaxy studied. Mass estimates from high-resolution stellar-, maser-, or gas-dynamics are probably accurate to a factor of two (Richstone et al., 1998; Gebhardt et al., 2000). Slightly less reliable (factor $\sim$2-5) estimates of $M_{\rm MDO}$ for large samples are possible using the tight correlation between central stellar velocity dispersion of the galaxy bulge (σ_c) and $M_{\rm MDO}$ (Merritt & Ferrarese, 2001; Gebhardt et al., 2000). In this paper we assume that the few $\times$ 10^{5-9} $M_\odot$ MDOs traced by dynamic methods are black holes, and interchangeably use the terms MDO and black hole. With the new MDO results the degeneracy between black hole mass and accretion rate when accounting for radiated luminosity is removed. Given AGN spectral energy densities and black hole masses in large samples of nearby AGNs, one can attempt to isolate factors which determine accretion rates and luminosities.

A weak correlation between the nuclear centimeter radio luminosity and the mass of the nuclear black hole has been found by several authors, e.g. Franceschini et al. (1998), Yi & Boughn (1999) and Di Matteo et al. (2001). This result has been used as evidence for the existence of an ADAF-like inflow since, in such a flow, the radio luminosity is predicted to scale with the black hole mass and the accretion rate (e.g. Mahadevan, 1997). Two significant weaknesses here are the low resolutions of the radio data, which allows significant contamination from other processes in the bulge, and the small sample sizes. Our 150 mas resolution radio observations of a large number of nearby LLAGNs considerably increase the number of LLAGNs with reliable black hole mass estimates *and* high resolution radio observations, allowing a better test of the relationship between the two quantities.

---

[1] The VLA and VLBA are operated by the National Radio Astronomy Observatory, a facility of the National Science Foundation operated under cooperative agreement by Associated Universities, Inc.

In the following sections we first define the samples used in the paper (Sect. 2), and report on new VLA and VLBA observations which complete our survey of the distance-limited ($\mathrm{D} \leq 19$ Mpc) sample of LLAGNs (Sects. 3 and 4). Observational results on radio-variability in LLAGNs are also presented in Sect. 4. In Sects. 5 to 8 we combine the new observations with those reported in the earlier papers in this series, and present comprehensive results on the radio properties of LLAGNs in the distance-limited ($\mathrm{D} \leq 19$ Mpc) sample, and their implications for the central engines in LLAGNs. In Sect. 9 we study the relationship between nuclear radio power and black hole mass, both for the distance-limited LLAGN sample and for the larger sample of nearby bright galaxies (most of them LLAGNs) defined in Sect. 2. The results are followed by a brief discussion (Sect. 10) on the nature of the central engines in LLAGNs.

2. Sample Selection

2.1. The LLAGN Sample

The results in this paper, and the new observations reported here, are based on LLAGNs selected from the Palomar spectroscopic survey of all (~ 470) northern galaxies with $\mathrm{B_T} < 12.5$ mag (Ho et al., 1995). Almost half of all galaxies in the Palomar survey host some form of LLAGN (Ho et al., 1997b). Spectroscopic parameters (including activity classification) of 403 galaxies in the Palomar sample have been presented in H97a, and from these we have chosen to study the 96 nearest ($\mathrm{D} \leq 19$ Mpc) LLAGNs – the "distance-limited LLAGN sample" – at 2 cm with the VLA at $\sim 0\farcs15$ resolution. The distribution of galaxy distance for the distance-limited LLAGN sample is shown in Fig. 1a. Clearly, biases arising from the distance distribution are expected to be small within this sample. Observations at 2 cm of 33 LLAGNs in the sample (taken in 1996 October) were presented in Nagar et al. (2000). New 2 cm observations of 72 LLAGNs in the sample are presented here (10 LLAGNs are in common between this work and Nagar et al. 2000, and 1 LLAGN [IC 356] was not observed).

Our VLA observations of the 95 LLAGNs resulted in the detection of 31 nuclei. Sixteen of these have core flux $\mathrm{S^{VLA}_{2cm}} > 2.7$ mJy, and all sixteen cores have a flat radio spectrum[2] ($\alpha \geq -0.3$, $\mathrm{S}_\nu \propto \nu^\alpha$). These sixteen objects - the "distance- and radio-flux-limited LLAGN sample", listed in Table 1, were chosen for further study at multiple frequencies with the VLA and at higher resolution with the VLBA. Multifrequency VLA observations of the nuclei in Table 1 (Nagar, Wilson, & Falcke 2001) and VLBA observations of roughly half of the nuclei in Table 1 have already been published (see column 5), while VLBA observations of the remaining seven nuclei in Table 1 are presented in the present paper.

2.2. The "MDO" Sample

In order to investigate the relationship between MDO mass and nuclear radio luminosity, we have expanded our distance-limited ($\mathrm{D} \leq 19$ Mpc) LLAGN sample as follows. We include 73 additional Seyferts and LINERs (at $\mathrm{D} > 19$ Mpc) from the list of LLAGNs in H97a; these have also been observed at 2 cm and 150 mas resolution (Nagar et al. 2000, Nagar et al., in preparation). Also, we include an additional 31 galaxies which have reliable MDO mass estimates published in the literature. These include all galaxies in Richstone et al. (1998), Gebhardt et al. (2000), Ferrarese & Merritt (2000), and Merritt & Ferrarese (2001), and individual galaxies from Shields et al. (2000) and Bower et al. (2000). Of the 200 galaxies, 154 have all three of the following: an estimated MDO mass (either directly from dynamic measurements or estimated from σ_c), a core radio flux, and a bulge luminosity. The distribution of galaxy distance for these 154 galaxies is shown in Fig. 1b.

3. New Observations and Data Reduction

3.1. VLA Observations and Data Reduction

Seventy two LLAGNs at $\mathrm{D} \leq 19$ Mpc were observed at 2 cm (15 GHz) with the VLA. The bulk of the new observations was carried out on 1998 March 3 and 1998 May 21 while the VLA was in A-configuration (Thompson et al., 1980) and on 1998 June 21 while the array configuration was being changed from A- to B-configuration. Data taken during the latter period have more or less the same resolution as A-configuration data as the outermost antennas of the array had not yet been moved. Six LLAGNs (IC 239, IC 1727, NGC 428, NGC 660, NGC 1055, and NGC 1058) were observed on 1998 July 31 while the array was in B-configuration and two LLAGNs (NGC 3941 and NGC 7177) were observed on 1998 September 5 and September 10, respectively, while the array was in A-configuration. Most of the data (all data taken before July 1998) were calibrated and mapped by HF and preliminary results have been presented in Falcke et al. (1999). The remaining data were calibrated and mapped by NN.

---

[2] In view of the non-simultaneity of the radio data used to derive the spectral index, we use $\alpha = -0.3$ instead of -0.5 as the cutoff between a steep and flat spectrum.

Data were calibrated and mapped using AIPS, following the standard reduction procedures as outlined in the AIPS cookbook[3]. Observations of 3C 286 and 0404+768 (for which we used a 2 cm flux-density of 1.46 Jy) were used to set the flux-density scale at 2 cm. For sources stronger than about 3 mJy, we were able to iteratively self-calibrate the data so as to increase the signal-to-noise ratio in the final map. The typical root mean square (r.m.s.) noise in the final maps was 0.2 mJy and we take the detection limit of the survey to be 1 mJy (i.e. $5\,\sigma$). The resolution of the final maps was $\sim 0\farcs15$ for the A-configuration maps and $\sim 0\farcs4$ for the B-configuration maps.

The 1σ error in flux bootstrapping (i.e. setting the flux density scale relative to the flux calibrators) is expected to be roughly 2.5%. Elevation dependent effects (atmospheric opacity and varying antenna performance with elevation) lead to additional errors when measuring the fluxes of some sources (see Sec. 4.2). Such elevation dependent effects are expected to be small for most sources as the flux calibrator sources were observed at elevations 45° to 50° and most sources were observed at elevations between 40° and 60°. We therefore did not correct for elevation dependent effects, but take them into account when estimating the error in the flux measurement.

3.2. VLBA Observations and Data Reduction

Nine of the sixteen nuclei listed in Table 1 have been previously observed with the VLBA or VLBI (see column 5), and new VLBA observations of the remaining seven are presented here. We also observed two additional LLAGNs (with $\mathrm{D} > 19$ Mpc) from the Palomar sample. The first, NGC 2655, has $\mathrm{S}^{\mathrm{VLA}}_{\mathrm{2cm}} > 2.7$ mJy, but does not have a flat-spectrum radio core (Nagar et al., 2000). The other, NGC 3147 has both $\mathrm{S}^{\mathrm{VLA}}_{\mathrm{2cm}} > 2.7$ mJy and a flat-spectrum radio core (Nagar et al. 2000, see also Ulvestad & Ho, 2001b).

These nine LLAGNs were observed at 6 cm (4.9 GHz) in a 10 hour VLBA run on April 1, 1999. Each source was observed at two different hour angles in order to obtain good (u, v)-coverage. At each hour angle, a cycle of 6.5 min on source + 1 min on a nearby phase calibrator was repeated four times. The total integration time on each source was therefore 52 minutes. The "fringe finder" sources 4C 39.25 and 3C 345 were also briefly observed, and a 7 minute observation of J1642+6856 was used to check (and correct) the amplitude calibration of the VLBA. The weather was fair (and dry) at all VLBA sites, except for occasional wind gusts in excess of 35 mph at Kitt Peak. There were a few intermittent tape problems at several antennas; all data points with tape weights less than 0.7 (on a scale of 0 to 1) were flagged as bad. Data were calibrated using AIPS, following the standard procedures outlined in chapter 9 of the AIPS cookbook. Bad (u, v) data were deleted before the phase solutions of the phase-calibrator observations were transfered to the galaxy data.

The sources were initially imaged using AIPS task IMAGR. For sources stronger than about 4 mJy, we were able to iteratively self-calibrate and image the data so as to increase the signal-to-noise in the final map. The self-calibration and imaging cycles were done using the DIFMAP package (Sheperd, 1997), and the final self-calibrated (u, v) files were then imaged using the AIPS task IMAGR. The peak flux-density of the source typically increased by a factor of 1.3 during the self-calibration process. Therefore, for sources weaker than 4 mJy, on which accurate self-calibration was not possible, we have multiplied the *peak* detected flux-density by 1.3 as a crude attempt to correct for atmospheric decorrelation losses. The r.m.s. noise in the final uniformly weighted images is typically 0.15 mJy to 0.2 mJy, and the resolution between 2 mas and 5 mas.

4. Observational Results

4.1. Results of the New VLA Observations

The results of the new VLA observations are listed in Table 2 with columns explained in the footnotes. All six LLAGNs observed in B-configuration ($0\farcs4$ resolution) were undetected. All remaining LLAGNs have been observed in A-configuration or at a resolution equivalent to that of the A-configuration (Sect. 3.1). Thus, the fluxes for all radio detected sources are measured at $\sim 0\farcs15$ resolution. The radio positions for the detected nuclei are limited by the positional accuracy of the phase calibrators, which is typically 2–10 mas, and by the accuracy of the Gaussian fit to the source brightness distribution, which depends on the signal to noise ratio of the source detection. The overall accuracy should typically be better than ~ 50 mas. We have compared the radio positions derived here with optical positions from Cotton, Condon, & Arbizzani (1999), which were measured from the digital sky survey with typical 1σ accuracy $1\farcs5$–$2\farcs5$ in each of right ascension and declination. The results (column 6 of Table 2) show a good ($\leq 2\sigma$) agreement in most cases.

Only two nuclei in Table 2, NGC 3628 and NGC 4486 (M 87), show reliable extended structure in our 2 cm maps. The extended emission in the starburst galaxy NGC 3628 is from a known star-forming region (Carral, Turner, & Ho, 1990) while that in NGC 4486 is from the well-known radio jet (e.g. Junor & Biretta, 1995). The absence of extended emission in the other nuclei is not surprising as the high resolution may resolve it out; in addition, such emission is expected to be weak at the high frequency observed. For a few sources, a Gaussian fit (with peak flux-density, major and minor axes as free parameters) to the nuclear radio source brightness distribution resulted in a Gaussian size slightly larger than the beam size so that the peak flux-density was slightly smaller than the total flux; however, the deconvolved source sizes were much smaller than half the beam size, so we consider these sources as unresolved. Thus, most of the detected 2 cm nuclear radio sources are compact at the $0\farcs15$ resolution (typically 15–25 pc) of our survey. The implied brightness temperatures for the 2 cm compact nuclei are typically $T_b \geq 10^{2.5-4.0}$ K.

---

[3] available online at www.nrao.edu

Non-simultaneous spectral indices for the 2 cm detected nuclei have been estimated by a comparison with radio data at other wavelengths from the literature (as indicated in column 12 of Table 2). While the actual value of the spectral index is uncertain given the resolution mismatch and the non-simultaneity of the observations, we can determine whether the core is flat spectrum ($\alpha \geq -0.3$; $S_\nu \propto \nu^\alpha$), or steep spectrum ($\alpha < -0.3$), as noted in column 11 of the table. We are confident of the reality of the flat spectra obtained for the following two reasons. Since compact flat-spectrum radio sources are often variable, the use of non-simultaneous data at two frequencies can cause some intrinsically flat-spectrum radio sources to be misclassified as steep-spectrum sources. However, since extended steep-spectrum radio sources are not variable, the use of non-simultaneous data at two frequencies should rarely cause intrinsically steep-spectrum radio sources to be misclassified as flat-spectrum sources. Also, since the resolution is better at the higher frequency, resolution effects will tend to steepen the measured spectrum if extended emission is present. Six of the 2 cm detected sources are not marked as flat-spectrum sources in the table. Of these, three show extended radio emission from jets or lobes - NGC 4388 (Falcke et al., 1998), NGC 4636 (Stanger & Warwick, 1986), and NGC 4472 (Ekers & Kotanyi, 1978), and one shows extended emission from star-formation - NGC 3628 (Carral, Turner, & Ho, 1990). This extended emission may dominate over any flat-spectrum nuclear component within the beam of our radio maps. For the two remaining sources, NGC 4293 and NGC 4419, VLA archive data at 6 cm ($0\farcs4$ resolution; peak flux-densities 4.1 mJy/beam and 11.8 mJy/beam, respectively) and 20 cm ($1\farcs2$ resolution; peak flux-densities 13.0 mJy/beam and 28.3 mJy/beam, respectively) show that both have steep-spectrum radio cores which are more or less unresolved at both frequencies.

4.2. Variability of the VLA-Observed Radio Emission

Except for a few well-studied cases, e.g. NGC 3031 [M 81] (Ho et al., 1999; Bietenholz et al., 2000) and NGC 5548 (Wrobel, 2000), little is known about radio variability in Seyferts and LLAGNs. In the course of our observations, we have observed several LLAGNs at multiple epochs using the same telescope (VLA), telescope configuration (A configuration), wavelength (2 cm), and data reduction methods (Nagar et al., 2000, 2001, Nagar et al., in preparation, this work). This offers us a unique opportunity to study radio variability in a sample of LLAGNs. Specifically, the 2 cm emission from all sixteen LLAGNs listed in Table 1 was observed at two epochs - March, May, or June 1998 (this work), and September 1999 (Nagar et al., 2001). The 2 cm emission from some of these sixteen LLAGNs was also observed in October 1996 (Nagar et al., 2000). The 2 cm emission from several other LLAGNs was also observed at these epochs. In addition, the 3.6 cm emission from the sixteen LLAGNs in Table 1 was observed in September 1999 (Nagar et al., 2001) and December 2000 (Nagar et al., in preparation).

The errors in the measured fluxes come from five significant factors (see the VLA Observational Status Summary for details[4]: (a) the accuracy of flux bootstrapping from a VLA 'flux' calibrator. The 3.6 cm fluxes at both epochs were bootstrapped from observations of 3C 286. The 2 cm fluxes were bootstrapped from observations of either 3C 286 and 0404+768 (for which we used a 2 cm flux-density of 1.46 Jy at all epochs). All VLA-recommended flux bootstrapping procedures were followed and the (1σ) errors due to this factor are estimated to be 1% at 3.6 cm and 2.5% at 2 cm. (b) variation of antenna gain with elevation. The gain of the VLA antennas at 2 cm and 3.6 cm is maximum at elevation $E_0 = 45°–50°$ and decreases (i.e. decreasing the estimate of the observed flux) as the elevation increases or decreases from E_0. At both epochs, all 3.6 cm observations were made at elevations 35°–70° with the flux calibrators observed at elevation ∼40°. The antenna gain variation over this elevation range is expected to be ≲0.3% and we therefore ignored this effect at 3.6 cm. The antenna gain variation at 2 cm is larger; it is less than 1.5% over the elevation range 35° to 65°, but increases to ∼4% at elevation 80°. The 2 cm flux calibrators were observed at elevations between 40° and 55° in all cases. The variation of gain with elevation was corrected for only in the reduction of the September 1999 data. For the other 2 cm data we took this effect into account when estimating the error of the flux determination. (c) atmospheric opacity. The atmospheric opacity at the VLA is typically 0.02 at 2 cm and ≲0.01 at 3.6 cm. At these opacities, atmospheric absorption will result in a source having an observed flux which is < 0.5% larger when observed at elevation 70° than at elevation 45°. We did not measure the atmospheric opacity during any of the observing runs except that of December 2000. From the weather conditions during the observing runs it is reasonable to assume the opacities were not significantly higher than the typical values quoted above. We did not correct for atmospheric opacity effects in the 2 cm and 3.6 cm data. Therefore, for sources observed at elevations below 45° we use the typical opacities above to estimate the additional error in the measured flux; It is notable that in the elevation range 45°-70° this effect works opposite to the effect discussed in (b), thus decreasing the overall error. (d) the r.m.s. noise in the final maps, which was typically 0.1 mJy and 0.2 mJy at 3.6 cm and 2 cm, respectively. (e) uncertainties intrinsic to the self-calibration process itself.

In summary, factor (a) usually dominates so that the 1σ flux calibration errors are typically about 1% and 2.5% for 3.6 cm and 2 cm observations at the VLA, respectively. While we have taken some effort to estimate the flux errors, other factors, e.g. variability in the flux calibrators, may cause the errors to be higher than estimated here, especially at 2 cm.

---

[4] www.nrao.edu

The inter-year variability for the LLAGNs with multi-epoch observations is shown in Fig. 2. We have plotted <S> versus ΔS/<S>, where ΔS is the r.m.s. flux variation and <S> the average flux (for nuclei with only two epochs of measurements, ΔS represents the difference between the fluxes). The grey shading delineates the region within which observed variability can be considered reliable. The lower cutoff to the shaded region is at 5 mJy. Sources with flux lower than this could not be accurately self-calibrated, which results in larger than usual errors in their flux determination. The left cutoff results from uncertainty in the flux-calibration. This uncertainty coupled with the r.m.s. noise in the radio maps could lead to values of ΔS/<S> which are $\sim 10\%$, even if the source did not vary. As an alternate illustration of the flux variability we have plotted the 2 cm 'light curves' for five of the nuclei in Fig. 3. In Fig. 3 the data for the first three epochs are from our 2 cm observations. The data for the last epoch shown (December 2000) has been obtained by scaling the previous epoch's 2 cm flux by the ratio of the 3.6 cm fluxes which were determined at both epochs.

As can be seen in the Figures, we find significant variability in almost half the sources. While the 2 cm flux values potentially suffer from significant flux calibration and elevation-dependent errors, the 3.6 cm flux-calibration is quite reliable. The result is made more credible by earlier observations of variability in NGC 3031 (Ho et al., 1999; Bietenholz et al., 2000) and NGC 4486 (Junor & Biretta, 1995). The large periods between the different epochs do not allow for detailed investigation of the variation, and at this point we are unable to find any clear correlation between the amount of variability and the other properties of the LLAGNs. Future higher time-resolution, multifrequency data will be useful in this context.

4.3. Results of the New VLBA Observations

All 7 objects from Table 1 which were newly observed with the VLBA at 6 cm were clearly detected in initial maps (i.e. without any form of self-calibration). Of the two other ($D > 19$ Mpc) LLAGNs observed, NGC 3147 was detected, but NGC 2655 was not detected at a 10σ limit of 0.76 mJy. The non-detection of NGC 2655 is not surprising as this object has a steep-spectrum radio core at arcsec resolution (Nagar et al., 2000). Of the detected nuclei, mas-scale radio cores were known to exist in NGC 4374 and NGC 4552 (e.g. Jones, Terzian, & Sramek, 1981). The results of the new VLBA observations are listed in Table 3, with columns explained in the footnotes. The source positions are referenced to the positions of their respective phase-calibrators. All phase calibrators were drawn from the VLBA calibrator survey and the positions we used at the time of observation were expected to be accurate to ±10 mas in each of R.A. and Dec. The phase calibrator positions have now been determined to an accuracy of 1 mas or better (Beasley et al., 2002) and the new positions are available on the web[5]. We therefore updated the positions of the sources to reflect the new accurate phase calibrator positions. The other factor contributing to the position uncertainty is the accuracy of the Gaussian fit to the source, which should typically be better than 2 mas. Thus the overall accuracy of the positions listed in Table 3 should be about 2 mas or better. The implied brightness temperatures were calculated using the formula given in Falcke et al. (2000); the results are in the range $10^{6.8}$ to $10^{9.5}$ K. Since most of the sources are unresolved, these values are lower limits to the true brightness temperatures.

Among the newly observed sources, the two with the highest peak flux-density at 6 cm, NGC 4374 (M 84) and NGC 4552 (M 89), clearly show extended structures (Fig. 4) suggestive of parsec-scale "jets." The pc-scale extension in NGC 4374 (detected earlier by Wrobel et al., 1996) is aligned with the larger kpc-scale FR-I radio lobes (e.g. Laing & Bridle, 1987), while the twin pc-scale extensions in NGC 4552 are, to our knowledge, the first time such structure has been detected in this galaxy. As pointed out in Nagar et al. (2001), of the sixteen objects in Table 1 the five with the highest 6 cm peak flux-densities at mas resolution – NGC 3031 (M 81; Bietenholz et al., 2000), NGC 4278 (Jones et al., 1984; Falcke et al., 2000), NGC 4486 (M 87; Junor & Biretta, 1995), NGC 4374 (M 84; Wrobel et al., 1996, this work), and NGC 4552 (M89; this work) – all have one- or two-sided pc-scale extensions, suggestive of jets. For these sources the peak flux-density of the extended emission is typically 10%–25% of the peak flux-density of the core. The signal-to-noise ratios of the core detections for the other eleven sources listed in Table 1 range between 10 and 50. The relative weakness of most of these sources does not allow very good self-calibration. This weakness, coupled with the low signal-to-noise expected for any extended component (10%–25% of a $10\,\sigma$–$50\,\sigma$ detection) may provide an explanation for the non-detection of weak extended structure in most of these sources. In fact, very deep VLBA observations of NGC 4258 reveal a sub-pc jet (Herrnstein et al., 1997).

5. Detection Rates of Radio Cores in the Distance-Limited Sample

5.1. Parsec-Scale Radio Cores (VLBA Detections)

The new VLBA results confirm that *all* LLAGNs at $D \leq 19$ Mpc with a 2 cm compact flat-spectrum core (as determined from VLA observations), i.e. 17% ±4% of all LLAGNs at $D \leq 19$ Mpc, have mas-scale radio cores with brightness-temperature $\gtrsim 10^8$ K. It is notable that this sample of LLAGNs with ultracompact radio cores is almost equally divided between Seyferts (6 of 16) and LINERs (8 of 16, see Table 1). Nuclear starbursts can have a maximum brightness-temperature of $\sim 10^{4-5}$ K

---

[5] www.nrao.edu

(Condon et al., 1991) while the most luminous known radio supernova remnants (e.g. Colina et al., 2001) would have brightness temperatures $\leq 10^7$ K even if they were $\leq$ 1 pc in extent. As argued in Falcke et al. (2000), if the core radio emission is attributed to thermal processes, the predicted soft X-ray luminosities of LLAGNs would be at least two orders of magnitude higher than observed by *ASCA* (Terashima, Ho, & Ptak, 2000) and *Chandra* (Ho et al., 2001). Finally, as discussed in Ulvestad & Ho (2001a), single SNRs (Colina et al., 2001) or a collection of SNRs (Neff & Ulvestad, 2000) would have radio spectral indices $\alpha \sim -0.7$ to -0.4 rather than the values $\alpha \sim -0.2$ to 0.2 seen in the VLBA-detected LLAGNs (Nagar et al., 2001). Thus, the only currently accepted paradigm which may account for the mas radio cores is accretion onto a supermassive black hole. In this case, the mas-scale radio emission is likely to be either emission from the accretion inflow (Narayan et al., 1998) or synchrotron emission from the base of the radio jet launched by the accreting supermassive black hole (Falcke & Biermann, 1999; Zensus, 1997).

Fifteen of the sixteen definite AGNs (Table 1) are either (a) type 2 LLAGNs in massive (M_B(total) ≤ -20) ellipticals (four galaxies), or (b) type 1 LLAGNs (two ellipticals and nine non-ellipticals). The remaining galaxy, NGC 5866, is a transition nucleus in an S0 galaxy with an ambiguous detection of broad Hα (H97c); the ambiguity is not unexpected as the dilution by H II regions in transition nuclei makes it more difficult to determine the presence of broad Hα than in "pure" LINERs and Seyferts (see H97c). NGC 5866 may, therefore, belong with the other nine type 1 non-ellipticals.

5.2. 100-Parsec-Scale Radio Cores (VLA Detections)

We have completed observations of 95 of the 96 LLAGNs in the distance-limited sample with the VLA; only IC 356, a transition nucleus, remains unobserved by us. IC 356 can be considered as a non-detection for our purposes since a significantly lower resolution (1′) flux measurement gives an upper limit of 2 mJy at 2.8 cm (Niklas et al., 1995).

When all 96 LLAGNs at D $\leq$ 19 Mpc are considered together, our VLA observations have detected 9 of 23 (39%) low-luminosity Seyferts[6], 16 of 37 (43%) LINERs, and 6 of 35 (17%) transition nuclei, at a resolution of $\sim 0\farcs15$ and above a flux limit of $\sim$ 1 mJy (Nagar et al. 2000; this work). Alternately, we can state that radio cores with luminosity $P^{\rm core}_{\rm 2cm} \geq 10^{20}$ W Hz^{-1} are found in 5 of 23 low-luminosity Seyferts, 8 of 37 LINERs, and 3 of 35 transition nuclei in the distance-limited sample. The radio luminosities of the detected 2 cm cores lie between 10^{18} and 10^{22} W Hz^{-1} (e.g. Fig. 5), similar to the luminosities seen in 'normal' E/S0 galaxies (Sadler et al. 1989). It is notable, however, that a significant fraction of the detected 2 cm compact cores are in spiral galaxies (Fig. 8a).

6. Correlations between Radio Power and Optical Emission-Line Properties in the Distance-Limited Sample

Emission-line fluxes and linewidths for the galaxies in the Palomar sample were typically measured over a $4'' \times 2''$ aperture centered on the galaxy nucleus (H97a). In this section we study the relationships between these nuclear emission-line properties and the core radio power measured at 150 mas resolution for LLAGNs in the distance-limited (D $\leq$ 19 Mpc) sample.

6.1. Emission-Line Luminosity

Correlations between the radio power and emission-line luminosity of active galaxies are well known, and are found in both Seyfert (de Bruyn & Wilson, 1978) and radio galaxies (Baum & Heckman, 1989). The [O III] λ5007 line is usually used in assessing these correlations, but this line is weak in LINERs and we use instead [O I] λ6300, which also has the advantage of being uncontaminated by emission from H II regions. In our D $\leq$ 19 Mpc LLAGN sample the 2 cm radio power appears approximately proportional to the nuclear [O I] λ6300 luminosity (Fig. 5), though there is a range of about two orders in magnitude of emission-line luminosity for a given radio power. Testing the statistical significance of the correlation is not straightforward as there are some uncertain values (non-photometric data) of the [O I] luminosities. For simplicity, we treat the non-photometric flux densities as photometric measurements when using the bivariate tests from the ASURV statistical software package (Lavalley et al., 1992, hereafter Asurv). This approximation should not bias the results significantly as the uncertainties of the non-photometric emission-line fluxes are expected to be a factor of only ±2 (H97a), which is small compared to the 3 orders of magnitude range of the [O I] luminosity. When this is done, the Asurv tests indicate that the [O I] luminosity is correlated with the 2 cm radio power at the 98.5%–99.9% significance level for the thirty-one 2 cm detected LLAGNs at D $\leq$ 19 Mpc, at the 99.9% significance level for all Seyferts and LINERs at D $\leq$ 19 Mpc, and at the 99.99% significance level for all 95 LLAGNs at D $\leq$ 19 Mpc which have been observed at 2 cm (see Table 4). The correlation among the radio-detected nuclei is not just a result of the elliptical galaxy nuclei having higher radio powers and emission-line luminosities than the non-ellipticals; among the 24 non-elliptical radio detections, the radio power and [O I] luminosity are correlated at the 99.5% significance (Table 4).

Interestingly, if we use the Hα+[N II] $\lambda\lambda$6548,6583 luminosity in place of the [O I] luminosity the data appear more scattered, and the significance of the correlation drops to 97%-98% for all radio detected LLAGNs and

---

[6] NGC 185 is considered a non-detection since the radio source detected in this galaxy is probably extra-nuclear (Nagar et al., 2000).

89%-93% for the radio-detected non-elliptical LLAGNs (Table 4).

6.2. Emission-Line Width

The only emission line for which the full width at half maximum (FWHM) is reported in the Palomar survey results is [N II] λ6583 (H97a). We therefore use this line for assessing the correlations between linewidths in LLAGNs and other parameters. For all radio detected nuclei considered together, all three of the [N II] λ6583 FWHM linewidth, [N II] λ6583 luminosity, and 2 cm radio power are correlated, with the significance of the correlations as follows: linewidth and radio power 99.9%, linewidth and [N II] luminosity 99-99.5%, and [N II] luminosity and radio power (97-99%; Table 4). The sample of low-luminosity Seyferts studied by Ulvestad & Ho (2001a) also follows the above three correlations at a high significance level. The [N II] linewidths of LINERs and transition nuclei are generally larger for the earlier type galaxies (the Seyferts do not show such a clear variation with morphological type). Also, the same early type galaxies tend to have higher radio powers though not necessarily higher [N II] luminosities. Interestingly, the [N II] linewidth does not show any clear dependence on the bulge or total magnitude of the galaxy among the LLAGNs with $D \leq 19$ Mpc.

That the galaxy rotation contributes to the [N II] linewidth is clear: the [N II] linewidth is correlated with the corrected (for galaxy inclination) rotational velocity of the host galaxy ($\Delta V^c_{\rm rot}$) for all LINERs (99.7% significance) and transition nuclei (97%-98% significance) with $D \leq 19$ Mpc (Fig. 6 and Table 4). The significance of the above correlation for only the radio detected LINERs is smaller (82%-95%) perhaps due to the small number of objects. More interestingly, there is evidence that the nuclear radio power is related to the ratio FWHM([N II])/$\Delta V^c_{\rm rot}$, which increases with increasing radio power (Fig. 7). This correlation has a significance of 99.9% if all radio detections are considered, and 98%-99% if only the non-elliptical radio detections are considered (Table 4). That this correlation may involve a direct physical significance is supported by the lack of a clear correlation between [N II] width and bulge luminosity among the LLAGNs with $D \leq 19$ Mpc. One immediate explanation for the correlation is that the radio source is responsible for "stirring" the [N II] emitting gas as is probably the case with powerful Seyferts (Wilson & Willis, 1980; Whittle, 1992b). The converse, however, is not true. That is, a high ratio of FWHM([N II])/$\Delta V^c_{\rm rot}$ does not necessarily imply a strong radio source: notice how the radio non-detections (Fig. 7b) show a large variation in the y-axis. This is one of the few suggestions that the radio non-detected nuclei are not simply lower radio-power versions of the radio detected nuclei. In both Figs. 6 and 7, the radio-detected nuclei NGC 4143, NGC 4168, NGC 4486, NGC 4552, and NGC 5866 are not plotted as these nuclei do not have values for the galaxy rotational velocity listed in H97a. The only three radio detected nuclei with [N II] linewidths in excess of $\Delta V^c_{\rm rot}$ (Figs. 6 and 7) are NGC 4278, NGC 4374 (both ellipticals with pc- to kpc-scale radio jets), and NGC 4772 which has a pc-scale radio core (Sect. 4.3).

7. Comparison of the Radio Detected and Non-Detected LLAGNs in the Distance-Limited Sample

The sixteen LLAGNs observed at mas resolution and discussed in Sect. 5.1 represent a flux-limited sample drawn from the 2 cm VLA-detected LLAGNs. It is likely that some fraction of the VLA-detected radio cores which have not yet been observed with the VLBA, and also some fraction of the VLA-non-detected LLAGNs, also have high-brightness temperature cores (and thus accreting black holes). These issues, crucial for determining the true incidence and properties of accreting black holes in nearby galaxies, are explored in the following sections. The fluxes and detection rates quoted in the following sections are those from the VLA survey.

7.1. LINERs and Low-luminosity Seyferts

The type 2 nuclei (broad Hα not detected) have a rather low VLA radio core detection rate: only 1 of 11 Seyfert 2 nuclei and only 8 of 27 LINER 2 nuclei are detected. The type 1 nuclei (broad Hα present) have a significantly higher detection rate: 8 of 10 LINER 1.9s, and 8 of 12 Seyfert 1s (1.0s to 1.9s) are detected at 2 cm. The difference between the detection rates of type 1s and type 2s increases when one considers the type classification more carefully. Of the 22 type 1 nuclei in the distance-limited sample, a definite detection (see Ho et al., 1997c) of broad Hα has been made in 17; the remaining five have probable detections of broad Hα. Also, 6 of the 38 LINER type 2 and Seyfert type 2 nuclei in the distance-limited sample have ambiguous (Ho et al., 1997c) detections of broad Hα. Of the definite type 1s, 13 of 17 (76%) are detected in the radio. The only four non-detected definite type 1s are NGC 2681, NGC 4051, NGC 4395, and NGC 4639. Excluding type 2s with an ambiguous detection of broad Hα, 7 of 32 (22%) type 2 LINERs and Seyferts are detected in the radio.

It is known that the radio powers of AGN are correlated with various parameters of the host galaxy, such as the bulge luminosity (e.g. Nelson & Whittle, 1996) and possibly the nuclear luminosity at optical/UV wavelengths (e.g. de Bruyn & Wilson, 1978; Baum & Heckman, 1989). It is, therefore, important to see if the preferentially higher detection rate of the type 1 nuclei over the type 2s is influenced by these effects. The single type 2 Seyfert detected in the radio, NGC 4472, is a massive (M_B(total) ≤ -20) elliptical. Of the eight type 2 LINERs detected in the radio, two (NGC 4374 and NGC 4486) are massive ellipticals, one (NGC 2841) has an ambiguous identification of broad Hα(H97c), four have very weak ($\sim$ 3-7 σ) radio detections and the last (NGC 4736, 1.9 mJy or $\sim 10\,\sigma$, distance

4 Mpc) is unusually nearby and would not be detected at the median distance of the sample. Turning to the type 1s, the two non-detected LINER 1.9s are NGC 2681 and NGC 4438. The former has among the lowest bulge luminosity, emission-line luminosities and [N II] FWHM in the LINER 1.9 sample, and the broad Hα detection is doubtful in the latter (H97c). The four non-detected Seyfert type 1s are NGC 3982, NGC 4051, NGC 4395, and NGC 4639. The broad Hα detection in NGC 3982 is doubtful (H97c) and the narrow Hα luminosity of NGC 4051 places it exactly on the operational cutoff between low-luminosity Seyferts and 'classical' Seyferts, so it may have a different type of central engine from LLAGNs. A sub-mJy mas-scale nuclear radio source with brightness temperature $> 2\times10^6$, potentially an accreting massive black hole, has been found in NGC 4395 (Wrobel, Fassnacht, & Ho, 2001). Such a weak radio core is expected in view of the extremely low bulge luminosity (M_B(total) $= -10.4$) of this galaxy. In summary, the radio-detected type 2s tend to be strong radio sources in high bulge luminosity galaxies or very weak radio sources, and of the six type 1 nuclei not detected in the radio, two have a doubtful detection of broad Hα and two have unusually low bulge luminosities which may be the reason for their radio non-detection. The preference for radio detected LLAGNs to be in type 1 nuclei is the only highly significant difference between the 2 cm detected and non-detected LINERs and Seyferts. Thus, it is most likely that the difference in radio power is indeed related to the AGN type.

In this context it is relevant to look at the detection rate of the elliptical LLAGNs at D $\leq$ 19 Mpc. All four massive (M_B(total) ≤ -20) type 2 ellipticals (one of which has a transition nucleus) and all three type 1 ellipticals (with M_B(total) values of -19.1, -18.9, and -20.7) have detected radio cores. Only three ellipticals (all type 2) remain undetected in the radio: NGC 185, NGC 3379, and NGC 4494. NGC 185 is a nearby very low bulge mass (M_B(total) $= -14.9$) elliptical and is thus expected to have a very low luminosity radio core; NGC 3379 (M_B(total) $= -19.4$) may actually be an S0 galaxy (Statler, 2001); NGC 4494 (M_B(total) $= -19.4$) has a very low emission-line luminosity (log $[L_{H\alpha}/W] < 30.54$; H97a). As noted above, the radio detection of the massive ellipticals would be expected if the radio power scales with the bulge luminosity in LLAGNs (Sect. 8.2). Among less massive ellipticals it may be that the type 1 nuclei are preferentially detected similar to the case for non-ellipticals.

Thus the demography of LLAGNs with VLA-detected radio cores is similar to that of the subset with VLBA-detected radio cores, i.e. radio cores are preferentially seen in either massive type 2 ellipticals or in type 1 LLAGNs. It is likely that we have detected 2 cm radio cores and broad Hα lines in only the more luminous LLAGNs, since the [O I] λ6300 luminosities of the Seyfert and LINER type 1 nuclei are higher than those of the type 2 nuclei at the 99.9% significance level. Ulvestad & Ho (2001a) arrived at a similar conclusion in their analysis of the radio powers of $\sim$ 45 Seyferts drawn from the Palomar sample. Further support for this idea comes from an apparent proportionality between core radio power and luminosity of the broad Hα component (Fig. 9a) for all (20) type 1.9s in the Palomar sample for which broad Hα luminosities were measured under photometric conditions (Ho et al., 1997c). Twelve of the plotted nuclei are in the distance-limited sample; radio data for the remaining nuclei were taken from Nagar et al. (in preparation). The proportionality is unlikely to be due to distance as it is also seen in the equivalent plot of fluxes (Fig. 9b).

Other marginally significant differences between the radio-detected and radio-non-detected nuclei include the following: as compared to the non-detected LINERs and Seyferts, the 2 cm detected LINERs and Seyferts have higher [O I] luminosities ($\sim$93% significance level; see Fig. 5), earlier morphological types (Fig. 8a), higher bulge luminosities (Fig. 10), and reside in regions with a higher galaxy density (90%–95% significance level; Fig. 8b). The galaxy density, from Tully (1988) and listed in H97a, is the density of all galaxies brighter than $M_B = -16$ mag in the vicinity of the object of interest. In other words, 50% of all 2 cm non-detected Seyferts and LINERs reside in galaxies which are located in regions of local galaxy density $< 0.5\,\mathrm{Mpc}^{-3}$, as compared to only 16% for 2 cm detected Seyferts and LINERs. The difference in the galaxy density is primarily a result of galaxies with more massive bulges being in regions of higher galaxy density: the three most massive ellipticals in the sample (all radio-detected) are at the centers of clusters ($\rho_{\rm gal} > 3$) while the four galaxies with the least massive bulges are in regions with $\rho_{\rm gal} < 1$. When these very high and very low bulge mass galaxies are excluded, the difference in galaxy densities between the detected and non-detected galaxies is no longer significant. A comparison of the ratio of radio to [O I] luminosity (Fig. 10) for radio detected and non-detected LLAGNs reveals that the ellipticals in the sample tend to have higher $L_{\rm rad}/L_{\rm [O\,I]}$ ratios than the non-ellipticals for both type 1 and type 2 nuclei. The highest ratios are in the most massive type 2 ellipticals. Our radio detection limits are not low enough to reveal any clear difference in this ratio between the radio detected and non-detected nuclei.

Most of the above factors are consistent with the idea that our radio observations have detected the more luminous LINERs and low-luminosity Seyferts, and that deeper radio observations of the sample will reveal a higher incidence of compact radio cores.

7.2. Transition Nuclei

The only[7] transition nucleus (out of 64 in the Palomar sample) which may have detected broad Hα emission is NGC 2985 (at D = 22.4 Mpc); this detection is doubtful (H97c). Thus it is most appropriate to compare transition nuclei to other type 2 LLAGNs in the sample. Although the detection rate of Seyferts and LINERs of both types is much higher than that of transition nuclei, the detection rate for type 2 LINERs and type 2 Seyferts (10/38 or 26%) is similar to that for all transition nuclei (6/35 or ∼ 17%). Asurv tests indicate that the 2 cm radio powers and the [O I] λ6300 luminosities of the transition nuclei are not significantly different from those of the type 2 LINERs and type 2 Seyferts. One way to test for a difference between the central engines of transition nuclei and other type 2 LLAGNs is to look for a systematic difference in the ratio of radio to [O I] λ6300 luminosities, since [O I] λ6300 is expected to trace the 'LINER' component rather than the star formation component. Our data do not show any clear difference (Fig. 10), but in view of the large number of upper limits to $\nu P_{\rm rad}$/[O I] λ6300 deeper radio imaging is required to address this issue. Not surprisingly (Sect. 7.1), if we compare the transition nuclei to both type 1 and type 2 LINERs and Seyferts, then Asurv tests indicate that the 2 cm radio powers of the transition nuclei are lower at the 99.5% significance level. The [O I] λ6300 luminosities of the transition nuclei are also lower than those of the Seyferts and LINERs in the sample at the 97%–99% significance level.

---

[7] NGC 1161, tentatively identified as a transition nucleus (H97a) and listed in H97c as having a definite broad Hα line is not in the Palomar sample (Ho et al., 1995).

Are there any clear differences between the 6 detected and the 29 non-detected transition nuclei? NGC 4552 is a massive elliptical and NGC 4419 and NGC 5866 have ambiguous identifications of broad lines (H97c) which may (see Sect. 7.1) be related to their radio core detections. Another likely factor is differences in the emission-line ratios (Fig. 11). The ratios plotted in Fig. 11 are used (e.g. Veilleux & Osterbrock, 1987) to distinguish between Seyferts, LINERs and H II-region type nuclei. The dotted lines show the spectral classification cutoffs used by H97a. Clearly the transition nuclei detected at 2 cm (filled squares) are preferentially found among transition nuclei which lie close to the LINERs and Seyferts in the plots (while the [N II]/Hα and [S II]/Hα ratios were not used for spectral classification it is clear that transition nuclei do not attain as high values of these ratios as LINERs and Seyferts). Two of the detected transition nuclei, NGC 3627 and NGC 3628, are an interacting pair, with the activity classification of NGC 3627 bordering on a Seyfert 2.0 (H97a). The classification of the elliptical NGC 4552 as a transition nucleus is uncertain as its Hβ flux is uncertain at the 30%–50% level (H97a). The median morphological type is $T^{\rm median} = 3$ for the undetected transition nuclei, while the detected transition nuclei have T values of -5, -1, 1, 3, 3 and 3. Finally, there are no significant differences in the [O I] luminosities and the local galaxy density between the detected and non-detected transitions. Therefore, it appears that the strongest factor which determines the probability of detecting a radio core in a non-elliptical transition nucleus is the proximity of its emission-line ratios to "pure" LINERs and Seyferts. This gives support to the view that at least some transition nuclei have both "pure" LINER/Seyfert and H II region components, with the detectability of the radio core determined by the strength of the former component. Filho et al. (2000) have detected arcsec-scale, 3.6 cm cores with a flat radio spectrum, in 5 of 25 transition nuclei from the Palomar spectroscopic sample (two of their five cores, NGC 3627 and NGC 4552, are also found to be compact and flat spectrum by us). They find that the detected transition nuclei are preferentially in early-type galaxies; our results are consistent with this.

7.3. H II *Nuclei*

While we have not investigated H II nuclei from the Palomar sample in the radio, it is instructive to check in what ways galaxies with H II region nuclei may differ from those with LLAGNs. As shown by Ho et al. (1997b), the H II nuclei in the Palomar sample are in later-type hosts as compared to the LLAGNs. This is also true for the subset of the Palomar sample at $D \leq 19$ Mpc. Further, the median absolute magnitude in the B-band of the bulge for the H II region galaxies at $D \leq 19$ Mpc ($M_{\rm B}^{\rm median}$(bulge) $= -16.83$) is significantly fainter than the equivalent median value for the low-luminosity Seyferts and LINERs at $D \leq 19$ Mpc ($M_{\rm B}^{\rm median}$(bulge) $= -18.65$). The median values have been obtained from the values of $M_{\rm B}$(bulge) listed in H97a. The differences between the $D \leq 19$ Mpc galaxies in the Palomar sample with H II nuclei and those with LLAGNs are thus deeper than just their nuclear spectral classification. Thus, while the H II region nuclei may also harbor accreting black holes, these will form a different population from those in LINERs, low-luminosity Seyferts, and transition nuclei.

8. The Influence of the Galaxy Bulge on the Properties of the Distance-Limited Sample

The bulge luminosity of the host galaxy is known to strongly influence the probability of finding a nuclear radio source in radio galaxies (Auriemma et al., 1977), and the power of the nuclear radio emission in early-type galaxies (Sadler et al., 1989). Further, for radio and Seyfert galaxies, the nuclear centimeter radio luminosity at arcsec-scales is correlated with the bulge luminosity over six orders of radio power (Nelson & Whittle, 1996). The bulge luminosity is also known to affect the nuclear emission-line luminosity in Seyfert galaxies (Whittle, 1992b), radio-galaxies (Zirbel & Baum, 1995), and even "normal" early-type galaxies (Sadler et al., 1989). In this section, we test whether the above relationships hold at the lower radio and emission-line luminosities of our sample of LLAGNs.

8.1. Emission-Line Luminosity

Among the radio detected nuclei, the [O I] λ6300 luminosity is not clearly related to the galaxy bulge magnitude (Fig. 12). Also, for $-17 > M_{\rm B}$(bulge) > -20 the radio detected nuclei and non-detected nuclei are fairly well mixed at any given bulge magnitude. It is only at the lowest and highest bulge magnitudes that all nuclei are undetected and detected in the radio, respectively.

Also shown in the figure are the low-luminosity extrapolations of the relationship between $L_{[\mathrm{O\,I}]}$ and M_B(bulge) for 'classical' Seyferts (dotted line; for these nuclei the [O III] λ5007 luminosity from Whittle (1992a) was converted to the [O I] luminosity using a factor of 0.04, typical of Seyferts (Veilleux & Osterbrock, 1987)) and an indicative line for FR I radio galaxies (dashed line; the total Hα+[N II] λλ6548,6583 luminosity from Zirbel & Baum (1995) was converted to an [O I] luminosity using a factor of 0.08, typical of the LINERs in our sample). Zirbel & Baum (1995) list total emission-line luminosities for radio galaxies; typically more than half of this luminosity is from the nuclear (<2.5 kpc) region (Baum & Heckman, 1989). It is notable that, while several Seyfert galaxies fall close to the low-luminosity extrapolation of 'classical' Seyferts, many lie much further away, the farthest being NGC 4168, NGC 4472 (both ellipticals), NGC 4565, and NGC 4725. The elliptical LINER with a high [O I] luminosity for its bulge magnitude is NGC 4278. The radio-detected Seyferts are indistinguishable from the other radio-detected LLAGNs and, when considered together, the radio-detected LLAGNs are closer to the low-luminosity extrapolation of FR I radio galaxies than to that of 'classical' Seyferts.

Since the Hα luminosity is often used to represent the emission-line luminosity for AGNs we now look at the dependence of this quantity on the galaxy luminosity (Fig. 13). The Hα+[N II] luminosity is significantly correlated with galaxy total luminosity separately for all ellipticals and all non-ellipticals in the Palomar sample (Fig. 13b; Table 4). Figure 13a suggests that, at a given galaxy bulge magnitude, the radio detected ellipticals (except for NGC 4278) have lower emission-line luminosities than the radio detected non-ellipticals, though the number of ellipticals is only 10. However, when the total galaxy luminosity is considered (Fig. 13b), the ellipticals and non-ellipticals detected in the radio fall more or less together, i.e. the galaxy total luminosity, rather than the galaxy bulge luminosity, appears to be a better predictor of the nuclear emission-line luminosity among radio detected LLAGNs. The low numerical significance of the statistical tests involving the radio-detected galaxies (Table 4) may simply reflect the small number of nuclei considered; the correlation between emission-line luminosity and galaxy bulge or total luminosity becomes significant when we also consider the 2 cm non-detections at $D \leq 19$ Mpc (Table 4, bottom). A linear fit to all radio-detected nuclei in Fig. 13 gives $L_{\mathrm{H}\alpha+[\mathrm{N\,II}]} \propto L_B^{0.43}$(total) and $\propto L_B^{0.26}$(bulge).

As with the [O I] luminosity, the Hα+[N II] luminosities of the LLAGNs fall closer to the low-luminosity extrapolation of FR I radio galaxies (Zirbel & Baum, 1995) than to that of 'classical' Seyferts (Fig. 13). The Hα+[N II] luminosities of the 'classical' Seyferts were derived by converting the [O III] λ5007 luminosities listed in Whittle (1992a) using standard emission-line ratios in Seyferts: $\mathrm{H}\alpha/\mathrm{H}\beta = 3.1$, $[\mathrm{O\,III}]\,\lambda5007/\mathrm{H}\beta = 10$, and $[\mathrm{N\,II}]\,\lambda6583/\mathrm{H}\alpha = 1$ (Veilleux & Osterbrock, 1987). As for the plot of $L_{[\mathrm{O\,I}]}$ vs M_B(bulge) given in Fig. 12, Fig. 13 shows that for a given galaxy total or bulge luminosity, the radio detected and radio non-detected galaxies have similar nuclear emission-line luminosities. It is only at the lowest and highest bulge luminosities that all galaxies are undetected and detected, respectively, in our radio survey.

8.2. Core Radio Power

The radio power of the radio-detected nuclei which are not in ellipticals does not depend on the galaxy total, bulge, or disk luminosity; linear fits in all cases give a line with approximately zero slope (Fig. 14). The upper limits to the radio emission of the undetected (small open symbols in Fig. 14) non-ellipticals strongly support this result. The few elliptical nuclei in the sample show a variation of 1 to 3 orders of magnitude in radio power for a given galaxy luminosity. The ellipticals in the sample generally have higher radio powers and higher galaxy luminosities than the non-ellipticals in the sample. Probably as a result of this, when all radio detected nuclei in the sample (i.e. both ellipticals and non-ellipticals) are considered together, the radio power is found to be correlated with the galaxy bulge luminosity (but not the galaxy total luminosity; Table 4), with linear fit $P^{\mathrm{core}}_{2\mathrm{cm}} \propto L_B^{1.1}$(bulge). The slope of this dependence is much shallower than that seen over 6 orders of magnitude of core radio power by Nelson & Whittle (1996) for both powerful radio (FR I and FR II) galaxies and Seyfert (type 1 and type 2) galaxies (dotted line in Fig. 14a; $P^{\mathrm{core}}_{2\mathrm{cm}} \propto L_B^{3.2}$(bulge)). It is also shallower than the relationship displayed by "normal" nearby elliptical and S0 galaxies[8] (the 30th percentile of the radio power rises as $L_B^{2.2}$; Sadler et al., 1989). Figure 14 shows that the core radio powers of LLAGNs are less than what would be expected from the low-luminosity extrapolations of more powerful AGNs. Factors which could affect the slopes and radio powers include the differences in the frequencies and resolutions between the various datasets. Given the longer wavelength (20 cm) and lower resolution ($1'' - 3''$) of the data used by Nelson & Whittle (1996) and Sadler et al. (1989), the nuclear radio emission is more likely to include emission from arcsec-scale radio jets and star-formation activity in the bulge in their data (see e.g. Sect. 11.2 of Whittle, 1992b) as compared to our higher resolution 2 cm data. High resolution radio observations, capable of isolating the flat spectrum pc-scale cores in the more powerful AGNs, are needed for comparison with our data.

---

[8] We used the relationships derived by Nelson & Whittle (1996) and Sadler et al. (1989) after changing H_0 to the value used in this paper and transforming their 20 cm luminosities to 2 cm assuming optically-thin synchrotron emission (spectral index −0.7). Both these transformations change the intercept of the line but not the slope.

8.3. The Interplay Between Core Radio Power and Emission-Line Luminosity

The interplay between radio and emission-line luminosity can be better understood in the context of the following two factors (discussed above): (1) for all LLAGNs considered together, the 2 cm core power ($\mathrm{P^{core}_{2cm}} \propto \mathrm{L_B^{1.1}}$(bulge)) increases more rapidly than the nuclear emission-line luminosity ($\mathrm{L_{H\alpha+[N\,II]}} \propto \mathrm{L_B^{0.26}}$(bulge)) with increasing bulge luminosity, as is also the case for "normal" elliptical and S0 galaxies (Sadler et al., 1989); (2) with increasing disk luminosity, the emission-line luminosity increases, but the radio power does not.

A plot of core radio power against Hα+[N II] $\lambda\lambda$6548,6583 luminosity for all LLAGNs at D $\leq$ 19 Mpc is shown in Fig. 15. This type of plot has been used to separate 'radio-loud' AGNs from 'radio-quiet' ones (e.g. Xu et al., 1999). Also plotted in the figure are the low-luminosity extrapolations of the same relationship for FR I and FR II radio galaxies from Zirbel & Baum (1995, dashed lines), and the sample of 'classical' Seyferts from Whittle (1992a, small triangles). The values quoted in these papers have been converted to a Hubble constant of 75 km s^{-1} Mpc^{-1}, and the Seyfert Hα+[N II] luminosities have been derived from the [O III] λ5007 luminosity as described in Sect. 8.1. Though there is considerable scatter, factor (1) above causes a general trend for high bulge-mass LLAGNs to occupy the top center of the plot and low bulge-mass LLAGNs to occupy the lower left. However, factor (2) allows many of the galaxies with low bulge luminosities to sit to the right of their compatriots with higher bulge luminosities by dint of their higher disk luminosities.

It is very interesting that most of the radio-detected LLAGNs fall in the region of Fig. 15 where the low-luminosity extrapolations of the radio-loud (FR I and FR II radio-galaxies) and radio-quiet (Seyfert galaxies from the compilation of Whittle, 1992a) nuclei intersect. There is thus no evidence for a radio-loud - radio-quiet divide in the LLAGNs. Most of the radio detected LINERs and transition nuclei are found close to the low-luminosity extrapolations of the FR I and FR II galaxies. Some of the LLAGNs are offset to higher emission-line luminosities from the FR I and FR II relationships. Essentially all of these LLAGNs are in disk-type galaxies, with disk gas probably contributing to the emission-line luminosity. The operational distinction between 'classical' Seyferts and low-luminosity Seyferts is $\log[(\mathrm{L_{H\alpha+[N\,II]}})/\mathrm{W}] \sim 33$, so it is not surprising that low-luminosity Seyferts near this luminosity fall near the low luminosity extrapolation of 'classical' Seyferts. It is notable in Fig. 15 that the elliptical galaxies tend to have a higher radio power at a given emission-line luminosity than the S0 or disk galaxies, as we already inferred from Fig. 10.

9. Radio Luminosity and Black Hole Mass

We now investigate the relationship between the nuclear radio luminosity and the mass of the nuclear black hole in nearby galaxies. When a direct measurement of the black hole mass from high spatial-resolution kinematic measurements (Richstone et al., 1998; Gebhardt et al., 2000) is not available, we use the relationship found by Merritt & Ferrarese (2001) between the black hole mass and the central stellar velocity dispersion, σ_c. Merritt & Ferrarese (2001) and Gebhardt et al. (2000, who used σ_e, the luminosity-weighted line-of-sight dispersion within the half-light radius) have shown that this relationship is very tight with its accuracy currently limited only by the measurement errors in σ_c and $\mathrm{M_{MDO}}$. Values of σ_c have been taken, in increasing order of preference, from the Lyon-Meudon Extragalactic Database (LEDA; Paturel et al., 1997), Prugniel et al. (1998) and its update in the 'Hypercat' database[9], Ferrarese & Merritt (2000) and Merritt & Ferrarese (2001). Ferrarese & Merritt (2000) and Merritt & Ferrarese (2001) list the value of σ_c after correction for aperture size. They find that the aperture corrections for the galaxies in their study are of order a few km s^{-1} except for some more distant ($\gtrsim$60 Mpc) galaxies. Therefore, since most of the galaxies we consider below are relatively nearby (typically $\leq$ 30 Mpc), we have not made any aperture corrections to the values of σ_c taken from other sources. In support of this, a comparison between the values of σ_c from Ferrarese & Merritt and those taken from LEDA or Hypercat agree to within 20% (Fig. 16). There is no evidence that the difference in the values of σ_c increases with galaxy distance or for later morphological types. However, the difference between the two estimates may increase with decreasing galaxy bulge luminosity (Fig. 16c).

In order to minimize confusion by radio emission from larger scale regions, e.g. jets/lobes or star formation in the bulge, we use mainly sub-arcsecond scale radio fluxes, and treat all radio flux measurements made at resolution $>$ 150 mas as upper limits to the 'core' radio flux. One may expect that even the $\leq$ 150 mas-resolution data (typically $\leq$ 15 pc) overestimates the flux from the central few hundred Schwarzschild radii. However, free-free and synchrotron self-absorption may be significant on sub-pc-scales, so the central flux could be significantly attenuated even at 2 cm (e.g. Ulvestad et al., 1999). Most of the measurements are made at frequencies of 15 GHz or higher and thus avoid some of the problems of contamination by radio outflows and star formation related processes. For the handful of measurements at frequencies lower than 15 GHz, we converted to estimated 15 GHz fluxes using a spectral index of 0, which is the median spectral index observed for mas-scale core radio emission in LLAGNs (Nagar et al., 2001). The lowest observed frequency we use is 1.4 GHz (20 cm); thus using a spectral index in the range ±0.7 instead of 0 would change the extrapolated 15 GHz flux by a factor of ≤ 5.

---

[9] http://www-obs.univ-lyon1.fr/hypercat/

9.1. Results for the Distance-Limited Sample of LLAGNs

The correlation between radio luminosity and bulge luminosity for LLAGNs has been explored in Sect. 8.2. The basic result is that the two quantities are correlated if all radio detections are considered together, but not when only non-elliptical galaxies are considered. The plot of radio luminosity vs. MDO mass (Fig. 17) also shows a strong correlation but considerable scatter. In fact the five massive ellipticals in the figure - NGC 4278, NGC 4374, NGC 4472, NGC 4486, and NGC 4552 - have very similar MDO masses ($\sim 10^9$ $M_\odot$) but widely different radio powers, even at mas resolution. This large spread does not necessarily imply a large spread in the radio luminosities within a few hundred R_s as there is evidence that the radio emission in all five of these sources is jet dominated (see Nagar et al., 2001).

9.2. Results for a Larger Sample of Nearby Galaxies

We now consider the interplay between radio power, MDO mass and bulge luminosity in the larger sample (Sect. 2.2) of relatively nearby galaxies. The core radio fluxes for the Seyferts and LINERs at $D >$ 19 Mpc in the Palomar sample were taken from Nagar et al. (2000) and Nagar et al. (in preparation). These are 150 mas resolution, 2 cm observations, like the observations of the $D \leq 19$ Mpc sample of LLAGNs. The core radio fluxes of the additional galaxies were taken from Carral, Turner, & Ho (1990), Condon et al. (1990), Crane (1979), Crane et al. (1993), Dhawan, Kellerman, & Romney (1998), Di Matteo et al. (2001), Fabbiano, Gioia & Trinchieri (1989), Feretti & Giovannini (1987), Franceschini et al. (1998), Gallimore, Baum & O'Dea (1997), Geldzahler & Fomalont (1984), Giovannini et al. (1998), Graham et al. (1981), Jones (1974), Jones & Wehrle (1997), Kellermann et al. (1998), Krichbaum et al. (1998), Laurent-Muehleisen et al. (1997), Nagar et al. (1999), Sadler et al. (1995), Slee et al. (1994), Trotter et al. (1998), Venturi et al. (1993), White et al. (1997), and Wrobel & Heeschen (1991). When kinematically-determined MDO masses were not available, we estimated the MDO mass from σ_c, as outlined in the previous sections. When available, distances have been taken from the same reference as that providing the black hole mass. Galaxy morphological types, corrected total magnitudes in the B band, and distances for the remaining galaxies have been taken from LEDA. All quantities were converted to the value of $H_0 - 75$ km s^{-1} Mpc^{-1} – used in this paper. In all, we found that 154 of these galaxies, 37 of which are ellipticals, have values for all three of the following: estimated MDO mass, core radio flux, and bulge luminosity. Sixty six of these 154 galaxies have a radio core detected at resolution better than 150 mas.

The nearby galaxies, spanning 9 orders of magnitude in radio power, 6 orders of magnitude in MDO mass, and 5 orders of magnitude in bulge magnitude, are plotted in Fig. 18[10]. With such a large range of values, it is clear that all three quantities are correlated. Asurv tests on all 154 galaxies and on only the 66 with radio cores at $\leq$ 150 mas resolution, indicate that the radio power is correlated with both the MDO mass and the bulge luminosity at the 99.99% significance level (Table 5). For our Galaxy, we plot the radio flux both at 10 mas resolution and at $\sim 10'$ (23 pc) resolution; the latter is well matched to the linear resolution for the other sources. At this matched resolution (which includes emission from the whole Sgr A complex), the Galaxy is no longer an outlier in the correlations.

Visually, the relationship between radio power and bulge luminosity appears to have less scatter than that between radio power and MDO mass, mainly because of the outliers in the latter: the massive ellipticals at the highest radio powers and NGC 3115. For $M_{\rm MDO} \simeq 10^{8.5-9}$, there is a range of a factor of 10^5 in $P_{\rm 2cm}$. We compare the correlations between the three variables using the Kendall τ coefficient. Numerically, $P_{\rm concordance}/P_{\rm discordance} = (1+\tau)/(1-\tau)$, where P is the probability. That is, $\tau = 1$ implies perfect concordance (i.e. perfect proportionality), $\tau = -1$ implies complete discordance (i.e. perfect inverse proportionality), and $\tau = 0$ implies an absence of correlation. If we consider all the galaxies in Fig. 18, the Kendall τ coefficient indicates that the closest correlation is between black hole mass and bulge luminosity (Kendall's $\tau = 0.53$), while the radio power is more or less equally correlated with the black hole mass ($\tau = 0.32$) and bulge luminosity ($\tau = 0.29$). The significance of all three correlations is 99.9% (Table 5). In order to determine the primary correlation between the three quantities (radio luminosity, black hole mass and bulge luminosity), we use a partial correlation analysis based on the Kendall τ coefficient (Akritas & Siebert, 1996). This method determines the partial correlation between the independent and dependent variables after taking away the influence of any correlation with a third (test) variable. We get similar results for both cases - partially correlating $M_{\rm MDO}$ and radio power with L(bulge) as the test variable (partial $\tau = 0.20$, significance 95%), and partially correlating L(bulge) and radio power with $M_{\rm MDO}$ as the test variable (partial $\tau = 0.16$, significance 95%). The presence of a 95% significance for the partial correlations indicates that the radio power is dependent on *both* the MDO mass and the bulge luminosity. This, however, is only a $\sim 2\,\sigma$ result. Thus, at this point, we cannot determine whether the radio power is primarily related to the black hole mass or the bulge luminosity or to both equally. A more conclusive analysis must await a better determination of the MDO versus σ_c relationship in lower mass ellipticals and in non-ellipticals.

---

[10] NGC 4278 has moved significantly between Figs. 17 and 18 as H97a use a distance of 9.7 Mpc while Richstone et al. (1998) use a distance of 17.5 Mpc, which is used in Fig. 18.

Among the 37 ellipticals the radio power is correlated with the bulge luminosity at the 98.5%-99.5% significance level and with the MDO mass at the 98.5%-99.8% level (Table 5). Linear regression analyses by the Buckley James method in Asurv yields:

$\log \mathrm{P}_{2\mathrm{cm}}^{\mathrm{elliptical}} = 2.33(\pm 0.67) \log \mathrm{L_B(bulge)} - 4.35$

$\log \mathrm{P}_{2\mathrm{cm}}^{\mathrm{elliptical}} = 2.11(\pm 0.63) \log \mathrm{M_{MDO}} + 2.33$

Here, and in the equations below, $\mathrm{P_{2cm}}$ is measured in Watt Hz^{-1}, $\mathrm{L_B}$ in solar luminosities, and $\mathrm{M_{MDO}}$ in solar masses.

For the 48 non-elliptical galaxies which are *detected* in the radio at resolutions better than 150 mas, the radio power is correlated with both the MDO mass and the bulge luminosity at the 99.99% with the following linear regression fits

$\log \mathrm{P}_{2\mathrm{cm}}^{\mathrm{detected\ S0/later}} = 1.92(\pm 0.27) \log \mathrm{L_B(bulge)} + 1.14$

$\log \mathrm{P}_{2\mathrm{cm}}^{\mathrm{detected\ S0/later}} = 1.15(\pm 0.21) \log \mathrm{M_{MDO}} + 11.35$

The presence of a few upper limits to the MDO mass and/or bulge luminosity among the non-elliptical galaxies which are not detected in the radio complicates the statistical tests. When both variables have upper limits to some data points, only the Schmitt binned regression can be used for linear fitting within the Asurv package. The results in this case are quite dependent on the number of bins chosen, e.g. for all galaxies with both MDO estimates and radio powers, $\mathrm{P_{2cm}} \propto \mathrm{M_{MDO}^{0.8}}$ when 5 bins are used, and $\mathrm{M_{MDO}^{0.6}}$ when 6 bins are used. We therefore delete the four nuclei with MDO mass upper limits and the three nuclei with upper limits to their bulge luminosities from the sample. Having done this, the Buckley James linear regression method gives the following for all (i.e. whether or not they are detected in the radio) non-elliptical galaxies:

$\log \mathrm{P}_{2\mathrm{cm}}^{\mathrm{all\ S0/later}} = 1.56(\pm 0.30) \log \mathrm{L_B(bulge)} + 2.85$

$\log \mathrm{P}_{2\mathrm{cm}}^{\mathrm{all\ S0/later}} = 1.07(\pm 0.21) \log \mathrm{M_{MDO}} + 10.52$

The standard deviations of the two relationships are similar for the ellipticals and non-ellipticals. Even though the linear regression gives a smaller slope for the non-ellipticals than the ellipticals in both relationships, this result is not certain given the large number of radio upper limits at the lower MDO masses and bulge luminosities. These data points could steepen the relationship for non-ellipticals and bring it closer to that for ellipticals. In fact, the current data show no contradiction to all of the galaxies being described by the same relationship. If we do this – i.e. fit ellipticals and non-ellipticals together – we get:

$\log \mathrm{P}_{2\mathrm{cm}}^{\mathrm{all}} = 1.89(\pm 0.21) \log \mathrm{L_B(bulge)} - 0.17$

$\log \mathrm{P}_{2\mathrm{cm}}^{\mathrm{all}} = 1.31(\pm 0.16) \log \mathrm{M_{MDO}} + 8.77$

if all galaxies are considered; and

$\log \mathrm{P}_{2\mathrm{cm}}^{\mathrm{radio\ core}} = 1.72(\pm 0.20) \log \mathrm{L_B(bulge)} + 3.15$

$\log \mathrm{P}_{2\mathrm{cm}}^{\mathrm{radio\ core}} = 1.14(\pm 0.16) \log \mathrm{M_{MDO}} + 11.49$

if only those galaxies with radio cores detected at resolution $\leq$ 150 mas are considered.

10. Discussion

For all 16 LLAGNs at $\mathrm{D} \leq 19$ Mpc observed at mas resolution (Sects. 4.3, 5.1) four factors point strongly to a non-thermal origin of their mas-scale radio cores: (1) the brightness temperatures at 6 cm are too high to be explained by thermal processes; (2) the morphologies of the five LLAGNs with extended mas-scale radio structure are suggestive of pc-scale "jets"; (3) the spectral shapes of the radio cores support a non-thermal origin for the radio emission (Nagar et al., 2001, 2002); and (4) significant flux variability is observed and is much more likely in non-thermal than thermal sources. Thus, the mas-scale radio emission is almost certainly related to accretion onto a massive black hole. The high-brightness temperatures of the cores and the presence of either a single component, or jet structures about a single bright component, make it likely that the radio cores we detect are within $\simeq$ 1 pc of the accreting black hole. If we are indeed looking directly at the accreting region or the base of the jet in the radio, then these nuclei are unique among nearby galaxies and merit further study in the radio.

The radio results imply that a large fraction (perhaps all) of LLAGNs have accreting massive black holes. If we consider only the mas detections, then at least 25% ± 6% of LINERs and low-luminosity Seyferts have accreting black holes. VLA-detected compact radio cores with flux <2.7 mJy were not investigated with the VLBA; in other respects these cores are similar to those with detected mas scale structure. Thus it is likely that *all* LLAGNs with VLA-detected compact radio cores (38% ± 8% of LINERs and low-luminosity Seyferts) have accreting black holes. The scalings between radio power, emission-line luminosity, and galaxy luminosity provide evidence that the radio non-detections are simply lower power versions of the radio detections. In fact we find no reason to disbelieve that *all* LLAGNs have an accreting black hole.

One of the most important results in this paper is that compact radio cores are found almost exclusively in massive ellipticals and type 1 LLAGNs. For massive ellipticals, the high bulge luminosity and black hole mass appear to be key factors related to the production of a radio core, in light of the scalings seen between radio power and these parameters. Among non-ellipticals, the preferential detection of type 1 LLAGNs may result from the limited sensitivity of optical and radio observations, which detect broad Hα and radio cores in only the more luminous LLAGNs. For example, it may be that type 1 LLAGNs are in an outburst phase, during which accretion power contributes significantly to the total nuclear power output, and during which they temporarily host both broad Hα emission and a compact radio core. This scenario is supported by the findings that the observed 2–10 keV luminosity in type 2 LLAGNs is insufficient to power the optical emission-lines unless the X-rays are heavily absorbed (Terashima, Ho, & Ptak, 2000), and that the nuclear UV emission in some type 2 LINERs, the far-UV component of which is responsible for powering the emission lines, is dominated by massive-star clusters (Maoz et al., 1998). As another alternative, one can invoke the unified scheme (Antonucci, 1993) and posit that all LLAGNs have accreting black holes and either (a) the radio emission in type 1 LLAGNs is beamed (weakly relativistic jets [$\gamma \sim 2$] can give boost factors of up to ~ 5) and/or (b) the 2 cm radio emission in type 2 LLAGNs is free-free absorbed by a 'torus' i.e. $\tau_{15\mathrm{GHz}} \geq 1$.

For the distance-limited ($\mathrm{D} \leq 19$ Mpc) sample of LLAGNs, we found (Sect. 8.3) that the emission-line luminosity increases with the galaxy disk luminosity, while the radio power is primarily correlated with the galaxy bulge luminosity. Thus doubling the bulge luminosity almost doubles the $\mathrm{P_{rad}/L_{emission-line}}$ ratio (Sect. 8, Figs. 5, 15). The lower bulge luminosity of late-type galaxies implies both a smaller radio power *and* a smaller $\mathrm{P_{rad}/L_{emission-line}}$ ratio than found for ellipticals. Thus with increasing total galaxy luminosity, the $\mathrm{P_{rad}/L_{emission-line}}$ ratio of elliptical and non-elliptical galaxy nuclei will become increasingly separated and can create a trend not unlike the 'radio-loud' and 'radio-quiet' sequences seen in more powerful AGNs (e.g. Xu et al., 1999).

In our larger, 'MDO' sample (Sect. 2.2), the radio power is correlated with both the estimated MDO mass ($\mathrm{P_{2cm}^{all}} \propto \mathrm{M_{MDO}^{1.3}}$) and the luminosity of the galaxy bulge ($\mathrm{P_{2cm}^{all}} \propto \mathrm{L_B^{1.9}(bulge)}$) over five or more orders of magnitude (Fig. 18). At this point it is not clear which of the two is the primary correlation. Partial correlation analysis suggests (at the $\sim 2\sigma$ level) that *both* correlations are physically significant. If so, the latter correlation could be due to the influence of the bulge mass on the accretion rate. More complete results must await a better characterization of the MDO versus σ_c relationship in low mass ellipticals and in non-ellipticals.

One model which may account for the correlation between radio power and black hole mass posits that the radio emission is thermal synchrotron radiation from the accretion inflow in an ADAF or CDAF type model. The approximate proportionality between these two quantities (Sect. 9.2) is consistent with the $\mathrm{L_{2\,cm}} \sim 3 \times 10^{36}\, M_7^{8/5}\, \dot{m}_{-3}^{6/5}$ ergs $\mathrm{s^{-1}}$ relationship expected in the ADAF model of Yi & Boughn (1999) for values of $\dot{m}$ $\sim 10^{-2}$ to $\sim 10^{-5}$ of the Eddington accretion rate. Here $\dot{m}_{-3} = \dot{m}/10^{-3}$, $\dot{m}$ is the mass accretion rate in units of the Eddington rate, and M_7 is $\mathrm{M_{MDO}}/10^7$. A strong argument against all the radio emission coming from an ADAF or CDAF is that many of the galaxies considered here show morphological evidence for pc-scale jets, have core radio spectra which are flatter than what is expected in simple ADAF or CDAF models (Nagar et al., 2001) and/or turn over in the 10-30 GHz range (Di Matteo et al. 2001; Nagar et al., in preparation, see Nagar et al. 2002). If a significant (perhaps dominant) component of the radio emission is from jets, then the data in Fig. 18 imply accretion rates much lower than $\sim 10^{-2} - 10^{-5}$ of the Eddington rate within an ADAF or CDAF type model.

In the context of a jet model, the correlations between core radio power and both black hole mass and galaxy bulge luminosity imply either (a) the strength of the pc-scale radio jet scales with the mass of the black hole, and/or (b) the radio emission from the pc-scale jet is influenced by the potential of the galaxy bulge. In the case of (a), if the radio power is linearly dependent on the black hole mass, as is consistent with Fig. 18, then (following the arguments of Ho, 2002) one can estimate the radio luminosity empirically from the bolometric luminosity ($\mathrm{L_{Bol}}$) of the AGN. This method implies that the nuclei with detected radio cores in Fig. 18 have $\mathrm{L_{Bol}/L_{Edd}} \sim 10^{-2}$ to 10^{-4}, with the linear fit to the radio detections (solid line in upper panel of Fig. 18) lying approximately at $\mathrm{L_{Bol}/L_{Edd}} \sim 10^{-3}$. The maximal jet model of Falcke & Biermann (1996) predicts that $\mathrm{P_{2cm}^{core}} \propto \dot{m}^{1.4}$: to fit the slope of the data in Fig. 18 this requires $\dot{m}$ to scale roughly linearly with $\mathrm{M_{MDO}}$, equivalent to requiring the LLAGNs to accrete at a roughly fixed fraction of the Eddington rate. If $\dot{m}$ does scale with $\mathrm{M_{MDO}}$ this model can reproduce the observed radio luminosities of the nuclei in Fig. 18 even for $\mathrm{L_{Bol}/L_{Edd}} \sim 10^{-3}$ (comparing Fig. 18 with Fig. 1 of Falcke & Biermann and assuming their $\mathrm{L_{disk}} \sim \mathrm{L_{Bol}}$).

In the context of (b) above, the relationship between radio power and black hole mass may come about indirectly as outlined below. The core radio power, at arcsec-scale resolution, is strongly correlated with the bulge magnitude over 6 orders of radio power for FR I and FR II radio galaxies, and Seyfert galaxies (Nelson & Whittle, 1996). For several reasons, powerful radio galaxies and luminous Seyfert galaxies are not posited to be powered by low-radiative-luminosity models, e.g. their derived accretion rates can be $\dot{m} \gtrsim 10^{-1.6}$, which is the currently believed upper limit for an ADAFs existence (Narayan et al., 1998), and they show rapid X-ray variability (e.g. Ptak et al., 1998). Thus, it is possible that some other factor is responsible for the scaling of the core radio power with the host galaxy bulge luminosity. This factor could be the mass loss rate of stars in the bulge, which should be related to both the black hole accretion rate and the pressure of the interstellar medium in the vicinity of the nucleus. A higher thermal pressure around the radio source would tend to confine it and enhance the radio power (cf. Nelson & Whittle, 1996). Alternatively, the correlation with black hole mass could be the primary one. As we have shown, the nearby galaxies we consider in Fig. 18 (lower panel) follow $\mathrm{P_{2cm}^{core}} \propto \mathrm{L_B^{1.9}(bulge)}$. Also the black hole mass scales with the bulge mass as $\mathrm{M_{MDO}} = 0.005\ \mathrm{M_{bulge}}$, where $\mathrm{M_{bulge}} = 2.5 \times 10^7\ (\mathrm{L_{bulge}}/10^9\,\mathrm{L_\odot})^{1.2}$ (Richstone et al., 1998). Combining these equations gives $\mathrm{P_{2cm}^{core}} \propto \mathrm{M_{MDO}^{1.6}}$. The slope of this relationship is exactly the same as that of the ADAF model of Yi & Boughn (1999) and is not too far from the behavior of the data in Fig. 18 (upper panel).

11. Conclusions

The completion of our radio survey of the 96 nearest ($\mathrm{D} \leq$ 19 Mpc) LLAGNs from the Palomar sample of nearby

bright galaxies has yielded the following main results:
a) All (16 of 16) of the LLAGNs investigated at mas resolution with the VLBA have pc-scale cores with brightness temperatures $\gtrsim 10^8$ K. The five of these nuclei with the highest core flux all have pc-scale jets. The luminosity, brightness temperature, morphology, and variability of the radio emission all argue against an origin in star-formation related processes or as thermal emission. Thus, the core radio emission probably originates either in an accretion inflow onto a supermassive black hole or from jets launched by this black hole-accretion disk system. The latter explanation is supported by the morphologies and spectra of the radio cores;
b) there is no reason to believe that the remaining LLAGNs with compact radio cores (investigated at 150 mas resolution) are different from the 16 LLAGNs investigated at mas resolution. Thus, at least half of all LINERs and low-luminosity Seyferts probably contain accreting black holes. The incidence for transition nuclei is much lower;
c) compact radio cores are preferentially found in massive ellipticals and in type 1 nuclei, i.e. nuclei in which broad Hα emission is present. For these nuclei, the core radio power is proportional to the broad Hα luminosity. The preferential detection of type 1 nuclei could result from: 1) observational selection effects, in which broad Hα and radio cores have been found only in the more powerful LLAGNs, 2) only the type 1 LLAGNs are bona-fide AGNs, or 3) within the unified scheme, type 1 nuclei are beamed and/or type 2 nuclei are free-free absorbed in the radio;
d) the radio power of the compact core is correlated with both the galaxy luminosity and the luminosity and width of the nuclear emission lines. These trends suggest that we have detected only the brighter LLAGNs, i.e. the true incidence of accreting black holes in LLAGNs is higher than indicated by our radio detections alone.
e) The core radio and nuclear emission-line properties of LLAGNs fall close to the low-luminosity extrapolations of more powerful AGNs, providing further support for a common central engine;
f) low-luminosity Seyferts and LINERs share many of the same characteristics in the radio. The transition nuclei detected are those which are the closest, in terms of emission-line diagnostic ratios, to Seyferts and LINERs. Thus at least some transition nuclei are really composite Seyfert/LINER + H II region nuclei, with the core radio power dependent on the Seyfert/LINER component;
g) with increasing bulge luminosity, the radio power increases more rapidly than the emission-line luminosity. Also, there is evidence that the disk luminosity of the galaxy is correlated with the nuclear emission-line luminosity (but not the core radio power). Both these factors contribute to a radio loud/quiet division between ellipticals and non-ellipticals at high bulge luminosities;
h) investigation of a sample of $\sim$150 nearby bright galaxies, most of them LLAGNs, shows that the nuclear ($\leq$150 mas) radio power is strongly correlated with both the estimated MDO mass and the galaxy bulge luminosity. Partial correlation analysis on the two correlations yields the result that each correlation is meaningful even after removing the effect of the other correlation. The nature of these important correlations is discussed. Low accretion rates ($\leq 10^{-2}$–10^{-3} of the Eddington rate) are implied in both ADAF- and jet-type models;
i) about half of all LLAGNs investigated show significant inter-year variability at 2 cm and 3.6 cm.
In short, all evidence points towards the presence of accreting black holes in a large fraction, perhaps all, of LLAGNs.

Acknowledgements. NN thanks Tim Heckman for valuable suggestions and corrections, and Alison Peck for help with the VLBA data reduction. We thank Loretta Gregorini for suggestions which improved the organization of the paper. This work was partially supported by the Italian Ministry for University and Research (MURST) under grant Cofin00-02-36 and the Italian Space Agency (ASI) under grant 1/R/27/00. Part of this paper is drawn from NN's thesis work at the University of Maryland, College Park.

References

Alonso-Herrero, A., Rieke, M. J., Rieke, G. H., & Shields, J. C. 2000, ApJ, 530, 688
Akritas, M. G. & Siebert, J. 1996, MNRAS, 278, 919
Antonucci, R. R. J. 1993, ARA&A, 31, 473
Auriemma, C., Perola, G. C., Ekers, R. D., Fanti, R., Lari, C., Jaffe, W. J., & Ulrich, M. H 1977, A&A, 57, 41
Barth, A. J., Filippenko, A. V., Moran, E. C. 1999, ApJ, 525, 673
Barth, A. J., Ho, L. C., Filippenko, A. V., & Sargent, W. L. W. 1998, ApJ, 496, 133
Bartel, N. et al. 1982, ApJ, 262, 556
Baum, S. A., & Heckman, T. M. 1989, ApJ, 336, 702
Baum, S. A., Zirbel, E. L., & O'Dea, C. P. 1995, ApJ, 451, 88
Beasley, A. J., Gordon, D., Peck, A. B., Petrov, L., MacMillan, D. S., Fomalont, E. B., & Ma, C. 2002, to appear in ApJS (astro-ph/0201414)
Begelman, M. C., Blandford, R. D., & Rees, M. J. 1984, Rev. Mod. Phys., 56, 255
Bietenholz, M. F., Bartel, N., Rupen, M. P., 2000, ApJ, 532, 895
Blandford, R. D. 1993, in Astrophysical Jets, ed. D. Burgarella, M. Livio, & C. P. O'Dea, (Cambridge: Cambridge Univ. Press), 15
Blandford, R. D., & Königl, A. 1979, ApJ, 232, 34
Bower, G. A., et al. 2000, BAAS, 197, 9203
Braatz, J., Wilson, A. S., & Henkel, C. 1997, ApJS, 110, 321
Carral, P., Turner, J. L., & Ho, P. T. P. 1990, ApJ, 362, 434
Colina, L., Alberdi, A., Torrelles, J. M., Panagia, N., & Wilson, A. S. 2001, ApJ, 553, L19
Condon, J. J., Cotton, W. D., Greisen, E. W., Yin, Q. F., Perley, R. A., Taylor, G. B., & Broderick, J. J. 1998, AJ, 115, 1693
Condon, J. J., Helou, G., Sanders, D. B., & Soifer, B. T. 1990, ApJS, 73, 359
Condon, J. J., Huang, Z.-P., Yin, Q. F., & Thuan, T. X. 1991 ApJ, 378, 65
Condon, J. J., & Yin, Q. F. 1990, ApJ, 357, 97

Cotton, W. D., Condon, J. J., & Arbizzani, E. 1999, ApJS, 125, 409

Crane, P. C. 1979, AJ, 84, 281

Crane, P. C., Cowan, J. J., Dickel, J. R., & Roberts, D. A. 1993, ApJ, 417, L61

de Bruyn, A. G., & Wilson, A. S. 1978, A&A, 64, 433

Dhawan, V., Kellerman, K. I., & Romney, J. D. 1998, ApJ, 498, L111

Di Matteo, T., Carilli, C. L., & Fabian, A. C. 2001, ApJ, 547, 731

Di Matteo, T., Quataert, E., Allen, S. W., Narayan, R., & Fabian, A. C. 2000, MNRAS, 311, 507

Dopita, M. A., & Sutherland, R. S. 1995, ApJ, 455, 468

Ekers, R. D. & Kotanyi, C. G. 1978, A&A, 67, 47

Fabbiano, G., Gioia, I. M., & Trinchieri, G. 1989, ApJ, 374, 127

Falcke, H. & Biermann, P. L. 1999, A&A, 342, 49

Falcke, H. & Biermann, P. L. 1996, A&A, 308, 321

Falcke, H., Nagar, N. M., Wilson, A. S., & Ulvestad, J. S. 2000, ApJ, 542, 197 (Paper II)

Falcke, H., Ho, L. C., Ulvestad, J. S., Wilson, A. S., & Nagar, N. M. 1999, International Symposium on Astrophysics Research and Science Education, ed. C. Impey, 223 (Notre Dame, Ind)

Falcke, H., Wilson, A. S., & Simpson, C. 1998, ApJ, 502, 199

Feretti, L., & Giovannini, G. 1987, A&A, 182, 15

Ferrarese, L, & Merritt, D. 2000, ApJ, 539, L9

Filho, M. E., Barthel, P. D., & Ho, L. C. 2000, ApJS, 129, 93

Filippenko, A. V., & Terlevich, R. 1992, ApJ, 397, L79

Fosbury, R. A. E., Mebold, U., Goss, W. M., & Dopita, M. A. 1978, MNRAS, 183, 549

Franceschini, A., Vercellone, S., & Fabian, A. C. 1998, MNRAS, 297, 817

Frank, J., King, A., & Raine, D. 1995, in Accretion Power in Astrophysics, 2nd edition, (Cambridge: Cambridge Univ. Press)

Freedman, W. L. et al. 1994, ApJ, 427, 628

Gallimore, J. F., Baum, S., A., & O'Dea, C. P. 1997, Nature, 388, 852

Garciá-Barreto, J. A., Rudnick, L., Franco, J., & Martos, M. 1998, AJ, 116, 111

Gebhardt, K., et al. 2000, ApJ, 539, L13

Geldzahler, B. J., & Fomalont, E. B. 1984, AJ, 89, 1650

Giovannini, G., Cotton, W. D., Feretti, L., Lara, L. & Venturi, T. 1998, ApJ, 493, 632

Graham, D. A., Weiler, K. W., & Wielebinski, R. 1981, A&A, 97, 388

Heckman, T. M. 1980, A&A, 87, 152

Heckman, T. M., Balick, B., & Crane, P. C. 1980, A&AS, 40, 295

Herrnstein, J. R., et al. 1999, Nature, 400, 539

Herrnstein, J. R., Moran, J. M., Greenhill, L. J., Diamond, P. J., Miyoshi, M., Nakai, N., & Inoue, M. 1997, ApJ, 475, L17

Ho, L. C. 2002, ApJ, 564, 120

Ho, L. C. 1999, ApJ, 516, 672

Ho, L. C. et al. 2001, ApJ, 549, L51

Ho, L. C., Filippenko, A. V., & Sargent, W. L. W. 1995, ApJS, 98, 477

Ho, L. C., Filippenko, A. V., & Sargent, W. L. W. 1997a, ApJS, 112, 315 (H97a)

Ho, L. C., Filippenko, A. V., & Sargent, W. L. W. 1997b, ApJ, 487, 568

Ho, L. C., Filippenko, A. V., & Sargent, W. L. W., & Peng, C. Y. 1997c, ApJS, 112, 391 (H97c)

Ho, L. C., van Dyk, S. D., Pooley, G. G., Sramek, R. A., & Weiler, K. W. 1999, ApJ, 118, 843

Jones, T. W. 1974, A&A, 30, 37

Jones, D. L., & Wehrle, A. E. 1997, ApJ, 484, 186

Jones, D. L., Terzian, Y., & Sramek, R. A. 1981, ApJ, 246, 28

Jones, D. L., Wrobel, J. M., & Shaffer, D. B. 1984, ApJ, 276, 480

Junor, W., & Biretta, J. A. 1995, AJ, 109, 500

Kellermann, K. I., Vermeulen, R. C., Zensus, J. A., & Cohen, M. H. 1998, AJ, 115, 1295

Koski, A. T., & Osterbrock, D. E. 1976, ApJ, 203, L49

Krichbaum, T. B., et al. 1998, A&A, 335, L106

Kukula, M. J., Pedlar, A., Baum, S. A., & O'Dea, C. P. 1995, MNRAS, 276, 1262

Laing, R. A., & Bridle, A. H. 1987, MNRAS, 228, 557

Laurent-Muehleisen, S. A., Kollgaard, R. I., Ryan, P. J., Feigelson, E. D., Brinkmann, W., & Siebert, J. 1997, A&AS, 122, 235

Lavalley, M., Isobe, T., & Feigelson, E. 1992, in Astronomical Data Analysis Software and Systems I, ed. D. Worrall, C. Biemesderfer & J. Barnes, (San Francisco: ASP), Vol. 25, 245 (Asurv)

Lovelace, R. V. E., & Romanova, M. M. 1996, in Energy Transport in Radio Galaxies, ed. P. E. Hardee, A. H. Bridle, & J. A. Zensus (San Francisco: ASP), Vol. 100, 25

Mahadevan, R. 1997, ApJ, 477, 585

Maoz, D., Filippenko, A. V., Ho, L. C., Rix, H.-W., Bahcall, J. N., Schneider, D. P., & Macchetto, F. D. 1995, ApJ, 440, 91

Maoz, D., Koratkar, A., Shields, J. C., Ho, L. C., Filippenko, A. V., & Sternberg, A. 1998, AJ, 116, 55

Melia, F. 1994, ApJ, 426, 577

Merritt, D. & Ferrarese, L. 2001, MNRAS, 320, L30

Mushotsky, R. F. 2000, BAAS, 196, 34.15

Nagar, N. M., Falcke, H., Wilson, A. S., & Ho, L. C. 2000, ApJ, 542, 186 (Paper I)

Nagar, N. M., Wilson, A. S., & Falcke, H. 2001, ApJ, 559, L87

Nagar, N. M., Wilson, A. S., Falcke, H., Ulvestad, J. S., & Mundell, C. G. 2002, in Issues in Unification of AGNs, Elba, Italy, May 2001, ed. R. Maiolino, A. Marconi, & N. Nagar, ASP Vol. 258 (astro-ph/0201156)

Nagar, N. M., Wilson, A. S., Mulchaey, J. S., & Gallimore, J. F. 1999, ApJS, 120, 209

Napier, P. J., Bagri, D. S., Clark, B. G., Rogers, A. E. E., Romney, J. D., Thompson, A. R., & Walker, R. C. 1994, Proc. IEEE, 82, 658

Narayan, R., Mahadevan, R., & Quataert, E. 1998, in The Theory of Black Hole Accretion Discs, ed. M. A. Abramowicz, G. Björnsson, & J. E. Pringle (Cambridge: Cambridge Univ. Press), 148

Narayan, R., Igumenshchev, I. V., & Abramowicz, M. A. 2000, ApJ, 539, 798

Neff, S. G., & Ulvestad, J. S. 1988, AJ, 96, 841

Neff, S. G., & Ulvestad, J. S. 2000, AJ, 120, 670

Nelson, C. H. & Whittle, M. 1996, ApJ, 465, 96

Niklas, S., Klein, U., Braine, J., & Wielebinski, R. 1995, A&AS, 114, 21

Osterbrock, D. E. 1981, ApJ, 249, 462

Osterbrock, D. E. 1989, Astrophysics of Gaseous Nebulae and Active Galactic Nuclei (Mill Valley, CA: Univ. Sci. Books)

Paturel, G., et al. 1997, A&AS, 124, 109 (LEDA)

Perlman, E. S., Biretta, J. A., Zhou, F., Sparks, W. B., & Macchetto, F. D. 1999, AJ, 117, 2185

Pringle, J. E. 1993, in Astrophysical Jets, ed. D. Burgerella, M. Livio, & C. P. O'Dea, (Cambridge: Cambridge Univ. Press), 1

Prugniel, P., Zasov, A., Busarello, G., & Simien, F. 1998, A&AS, 127, 117

Ptak, A., Yaqoob, T., Mushotzky, R., Serlemitsos, P., & Griffiths, R. 1998, ApJ, 501, L37

Rees, M. J., Begelman, M. C., Blandford, R. P., & Phinney, E. S. 1982, Nature, 295, 17

Richstone, D., et al. 1998, Nature, 395A, 14

Roberts, T. P., & Warwick, R. S. 2000, MNRAS, 315, 98

Roy, A. L., Norris, R. P., Kesteven, M. J., Troup, E. R., & Reynolds, J. E. 1998, MNRAS, 301, 1019

Sadler, E. M., Jenkins, C. R., & Kotanyi, C. G. 1989, MNRAS, 240, 591

Sadler, E. M., Slee, O. B., Reynolds, J. E., & Roy, A. L. 1995, MNRAS, 276, 1373

Sanghera, H. S., Saikia, D. J., Luedke, E., Spencer, R. E., Foulsham, P. A., Akujor, C. E., & Tzioumis, A. K. 1995, A&A, 295, 629

Shepherd, M. C. 1997, in Astronomical Data Analysis Software and Systems VI, A.S.P. Conference Series, ed. Hunt, G. & Payne, H. E., (San Francisco: ASP) Vol. 125, 77

Shields, J. C. 1992, ApJ, 399, L27

Shields, J. C., et al. 2000, ApJ, 534, L27

Simien, F., & de Vaucouleurs, G. 1986, ApJ, 302, 564

Slee, O. B., Sadler, E. M., Reynolds, J. E., & Ekers, R. D. 1994, MNRAS, 269, 928

Smith, H. E., Lonsdale, C. J., & Lonsdale, C. J. 1998, ApJ, 492, 137

Sramek, R. 1992, in Relationships between Active Galactic Nuclei and Starburst Galaxies, ed. A. V. Filippenko (San Francisco: ASP), Vol. 31, 70

Stanger, V. J. & Warwick, R. S. 1986, MNRAS, 220, 363

Statler, T. S. 2001, AJ, 121, 244

Storchi-Bergmann, T., Eracleous, M., Livio, M., Wilson, A. S., Filippenko, A. V. & Halpern, J. P. 1995, ApJ, 443, 617

Terashima, Y., Ho, L. C., & Ptak, A. F. 2000, ApJ, 539, 161

Terlevich, R., & Melnick J. 1985, MNRAS, 213, 841

Terlevich, R., Tenorio-Tagle, G., Franco, J., & Melnick, J. 1995, MNRAS, 272, 198

Thompson, A. R., Clark, B. G., Wade C. M., & Napier, P. J. 1980, ApJS, 44, 151

Trotter, A. S., Greenhill, L. J., Moran, J. M., Reid, M. J., Irwin, J. A., & Lo, K. 1998, ApJ, 495, 740

Tully, R. B. 1998, Nearby Galaxies Catalog (Cambridge and New York: Cambridge University Press)

Ulvestad, J. S. & Ho, L. C. 2001, ApJ, 558, 561

Ulvestad, J. S. & Ho, L. C. 2001, ApJ, 562, L133

Ulvestad, J. S., & Wilson, A. S. 1984a, ApJ, 278, 544

Ulvestad, J. S., & Wilson, A. S. 1984b, ApJ, 285, 439

Ulvestad, J. S., & Wilson, A. S. 1989, ApJ, 343, 659

Ulvestad, J. S., Wrobel, J. M., Roy, A. L., Wilson, A. S., Falcke, H., & Krichbaum, T. P. 1999, ApJ, 517, L81

van der Marel, R. P. 1999, AJ, 117, 744

Veilleux, S. & Osterbrock, D. 1987, ApJS, 63, 295

Venturi, T., Giovannini, G., Feretti, L., Comoretto, G., & Wehrle, A. E. 1993, ApJ, 408, 81

Vila, M. B., Pedlar, A., Davies, R. D., Hummel, E. & Axon, D. J. 1990, MNRAS, 242, 379

White, R. L., Becker, R. H., Helfand, D. J., & Gregg, M. D. 1997, ApJ, 475, 479 (FIRST)

Wilson, A. S. & Willis, A. G. 1980, ApJ, 240, 429

Whittle, M. 1992a, ApJS, 49, 79

Whittle, M. 1992b, ApJ, 387, 121

Wrobel, J. M. 2000, ApJ, 531, 716

Wrobel, J. M., Fassnacht, C. D., & Ho, L. C. 2001, ApJ, 553, L23

Wrobel, J. M., & Heeschen, D. S. 1984, ApJ, 287, 41

Wrobel, J. M., & Heeschen, D. S. 1991, AJ, 101, 148

Wrobel, J. M., Walker, R. C., & Bridle, A. H. 1996, in Extragalactic radio sources: proc. of the 175th Symposium of the IAU, ed. R. D. Ekers, C. Fanti, & L. Padrielli (Kluwer Academic Publishers), 131

Xu, C., Livio, M., & Baum, S. 1999, AJ, 118, 1169

Yi, I., & Boughn, S. P. 1999, ApJ, 515, 576

Zensus, J. A. 1997, ARA&A, 35, 607

Zirbel, E. L., & Baum, S. A. 1995, ApJ, 448, 521

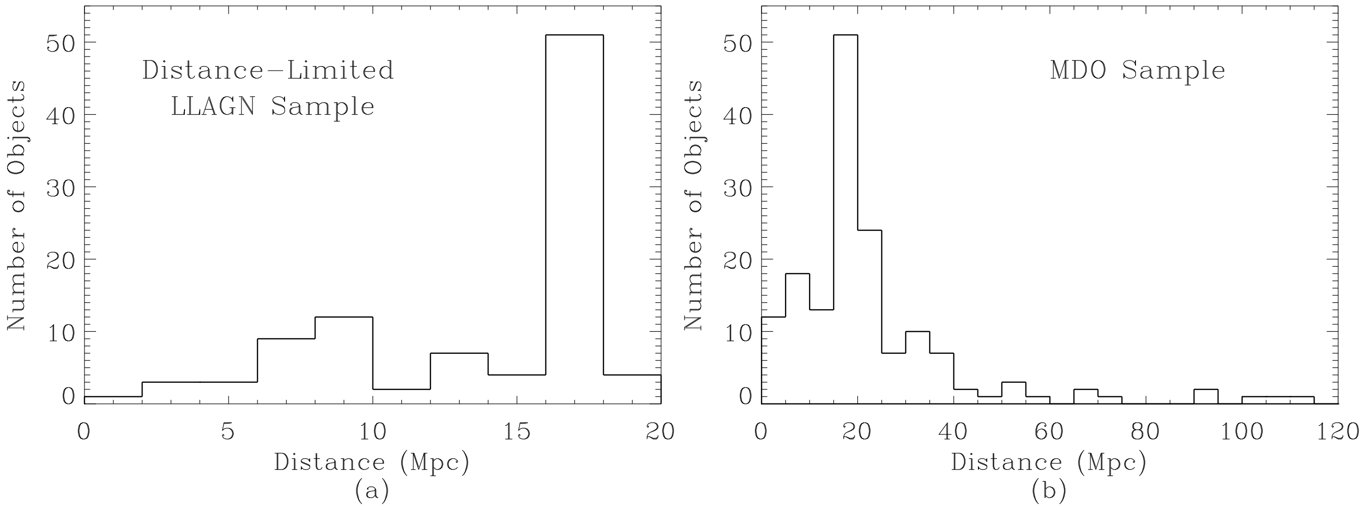

Fig. 1. Histograms of the galaxy distance for the **(a)** distance-limited (D ≤ 19 Mpc) LLAGN sample, and **(b)** MDO sample. Virgo cluster members create the peak at D ∼ 17 Mpc.

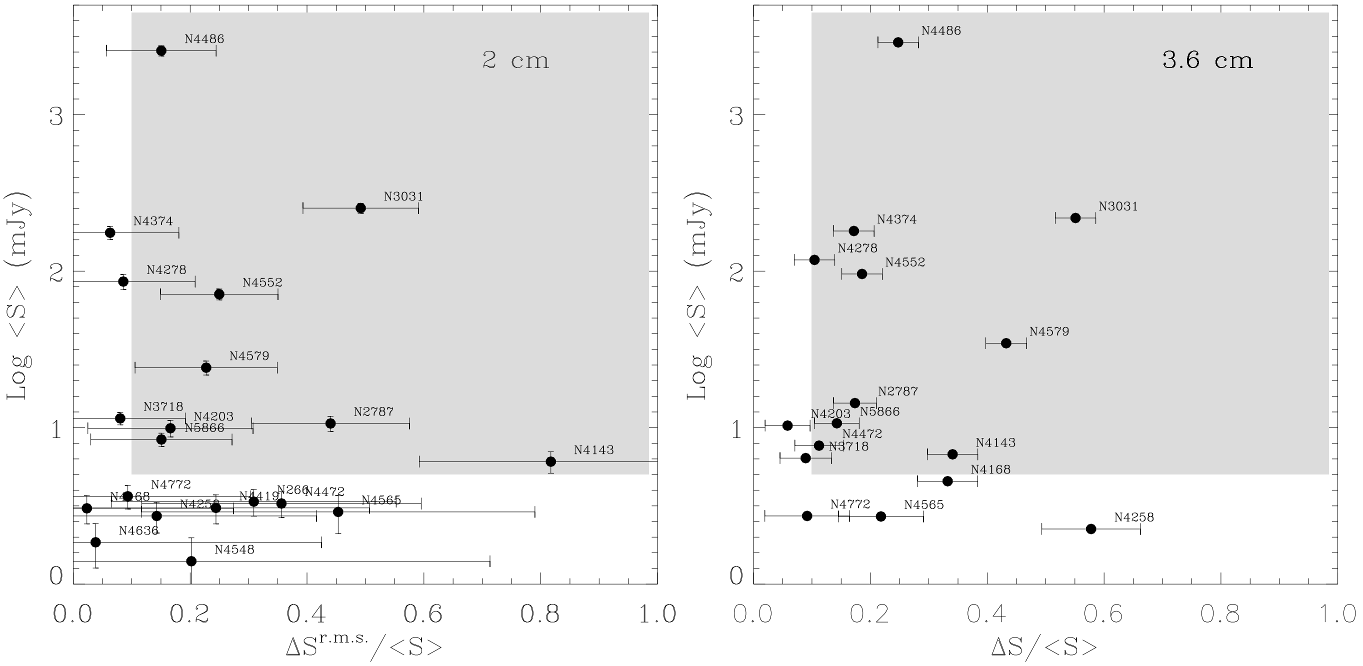

Fig. 2. The inter-year variability of the nuclear **(left)** 2 cm flux, and **(right)** 3.6 cm flux, in LLAGNs. The Y axis is the logarithm of the average measured flux, and the X axis is the r.m.s. of the flux variation about the average flux divided by the average flux. For the 3.6 cm data, and a few 2 cm datapoints, only two epochs are available and for these cases ΔS represents the difference of the two flux values. Estimated $\pm 2\,\sigma$ errors in X and Y are shown. When error bars in Y are not shown, they are smaller than the plot symbol. Points outside the shaded area are likely to be dominated by errors in flux-calibration and/or radio imaging (see text); these points are therefore not reliable.

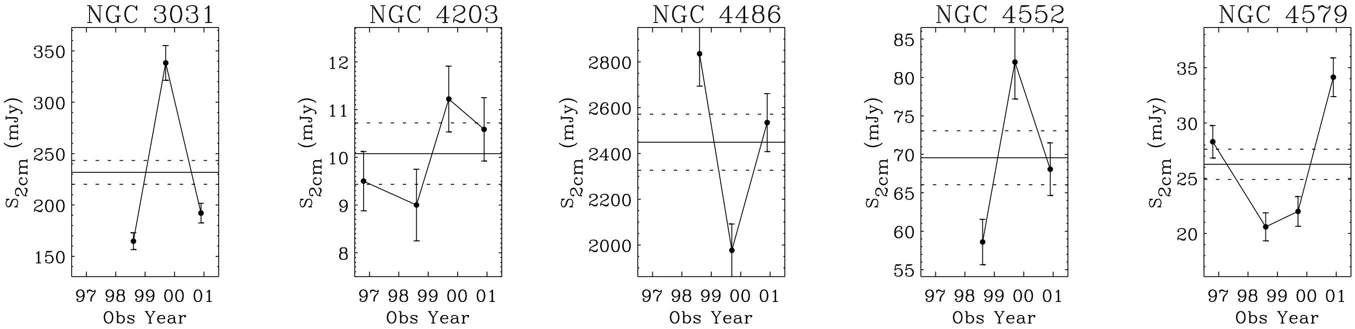

Fig. 3. 2 cm light curves for five of the LLAGNs in Fig. 2. The 2 cm flux at the last epoch (December 2000) has been obtained by scaling the previous epoch's 2 cm flux by the ratio of the 3.6 cm fluxes, which were obtained on both epochs. Estimated $\pm 2\,\sigma$ error bars (from flux calibration and mapping errors) are shown for each datapoint. In each panel the horizontal solid line shows the average flux over the observed epochs and the dashed lines show the estimated $\pm 2\,\sigma$ errors for the average flux value.

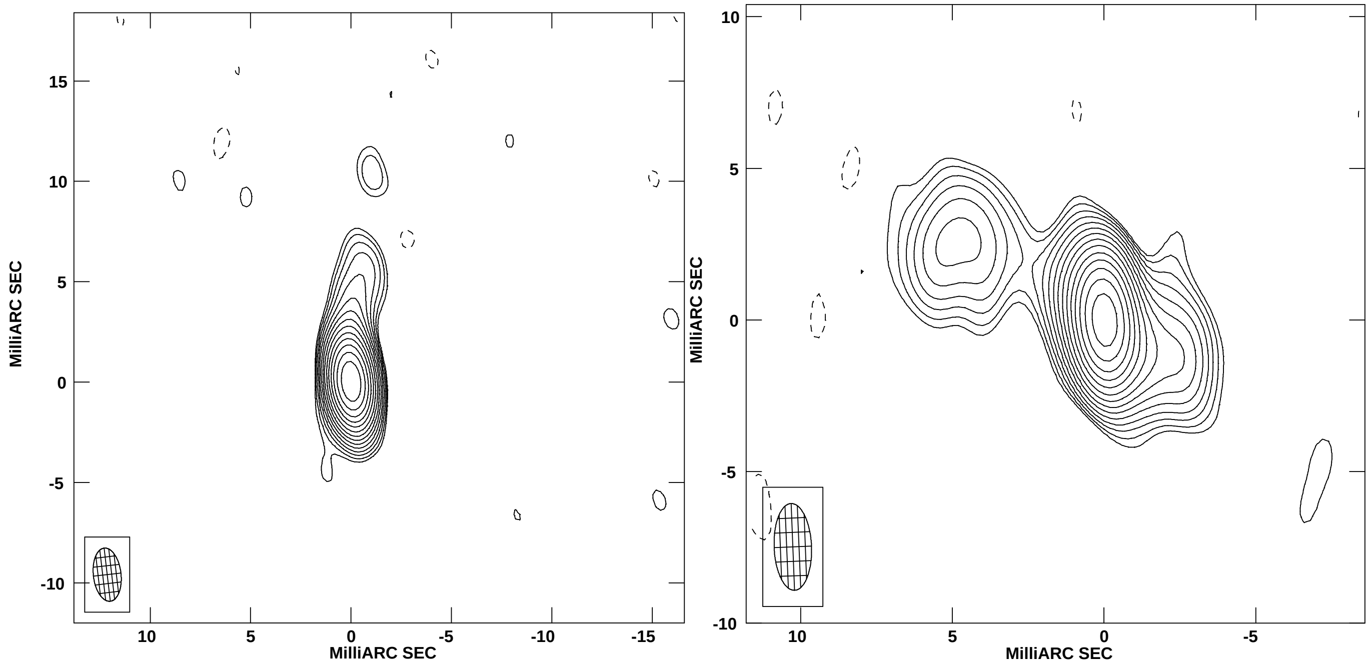

Fig. 4. 5 GHz (6 cm) VLBA maps of NGC 4374 **(left)** and NGC 4552 **(right)**. The contours are integer powers of $\sqrt{2}$, multiplied by the $\sim\ 3\,\sigma$ noise level of 1.2 mJy for NGC 4374, and by the $\sim\ 2\,\sigma$ noise level of 0.8 mJy for NGC 4552. The peak flux-densities are 152.6 mJy/beam and 93.8 mJy/beam, respectively.

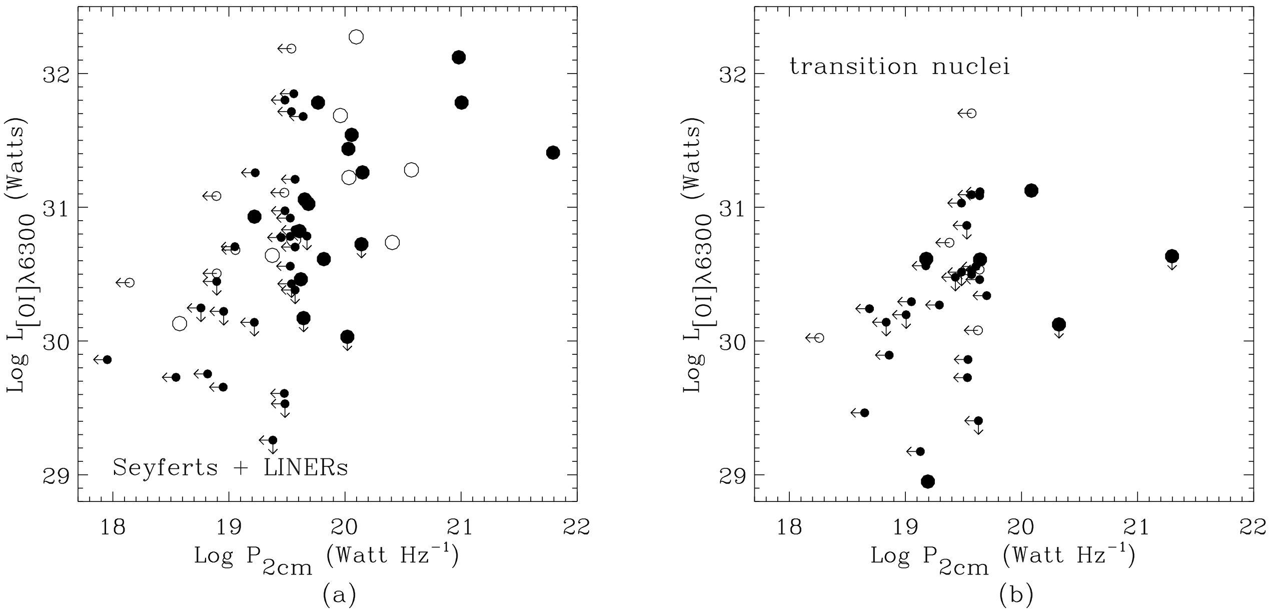

Fig. 5. Relationship between [O I] λ6300Å luminosity and 2 cm core (150 mas resolution) radio power for **(a)** all LINERs and low-luminosity Seyferts, and **(b)** all transition nuclei, in the distance-limited (D ≤ 19 Mpc) sample. Large symbols are used for radio detections. Objects with non-photometric [O I] λ6300Å flux measurements are shown as open circles.

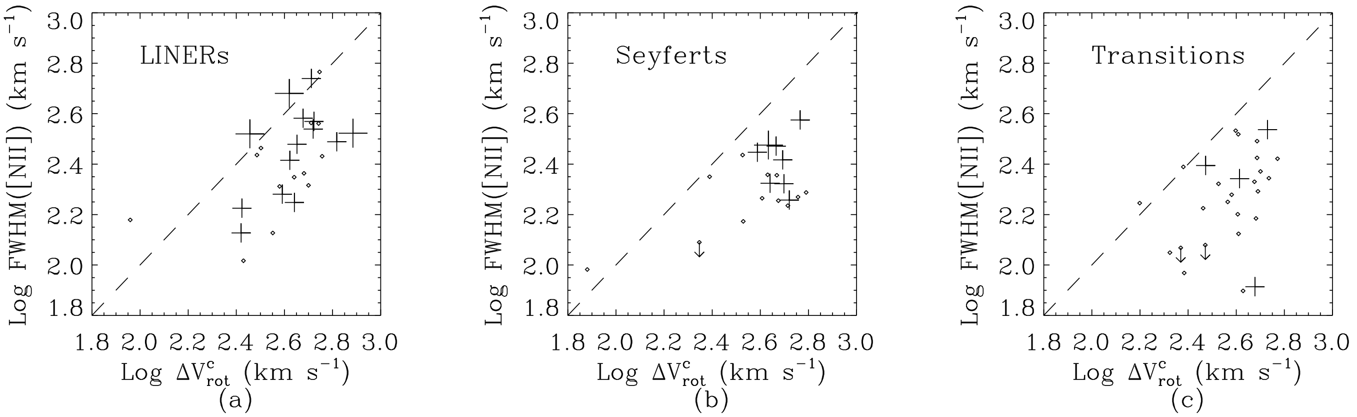

Fig. 6. Relationship between the FWHM of the nuclear [N II] λ6583 emission-line (as listed in H97a) and the inclination-corrected rotational velocity of the galaxy ($\Delta V^{c}_{\rm rot}$; as listed in H97a) for **(a)** LINERs, **(b)** Seyferts, and **(c)** transition nuclei, in the distance-limited (D ≤ 19 Mpc) sample. Radio-detected ellipticals are shown with large crosses, radio-detected non-ellipticals with small crosses, and all radio non-detections with dots.

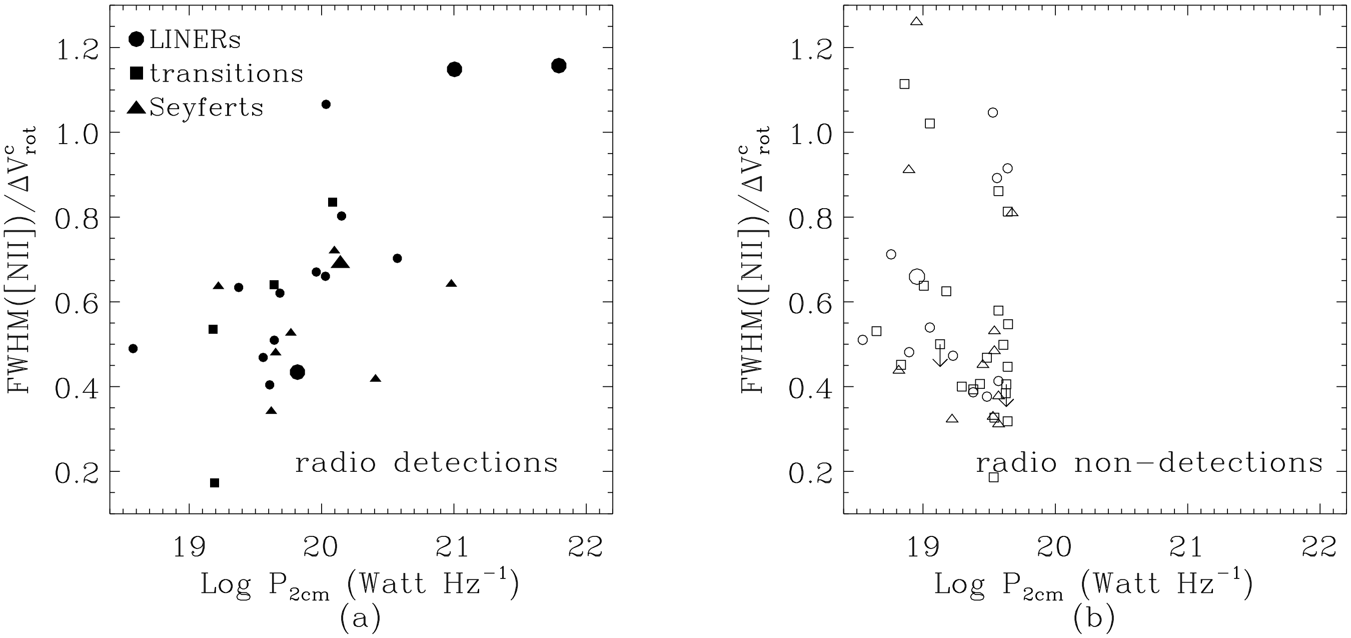

Fig. 7. Relationship between the ratio of the FWHM of the nuclear [N II] λ6583 emission-line to the inclination corrected rotational velocity of the galaxy and the 2 cm core (150 mas resolution) radio power for **(a)** radio detected nuclei and **(b)** radio non-detected nuclei in the distance-limited (D ≤ 19 Mpc) sample. Large symbols are used for elliptical galaxies and filled symbols for radio detections. The symbols in the right panel thus represent upper limits to the radio power.

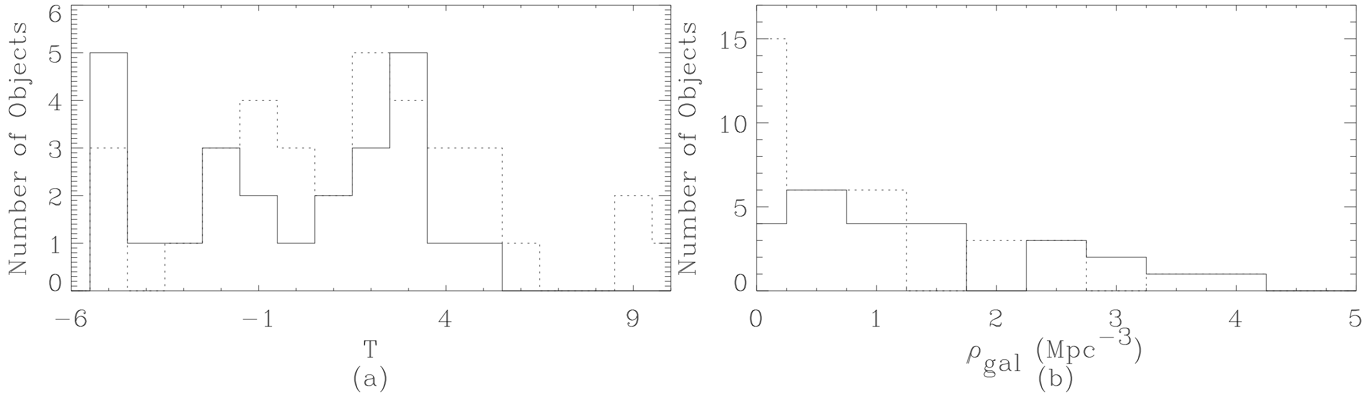

Fig. 8. Histograms of **(a)** the galaxy morphological type, and **(b)** the local galaxy density, comparing the D ≤ 19 Mpc LLAGNs detected at 2 cm (solid lines) and those not detected at 2 cm (dotted lines). All values are as listed in H97a.

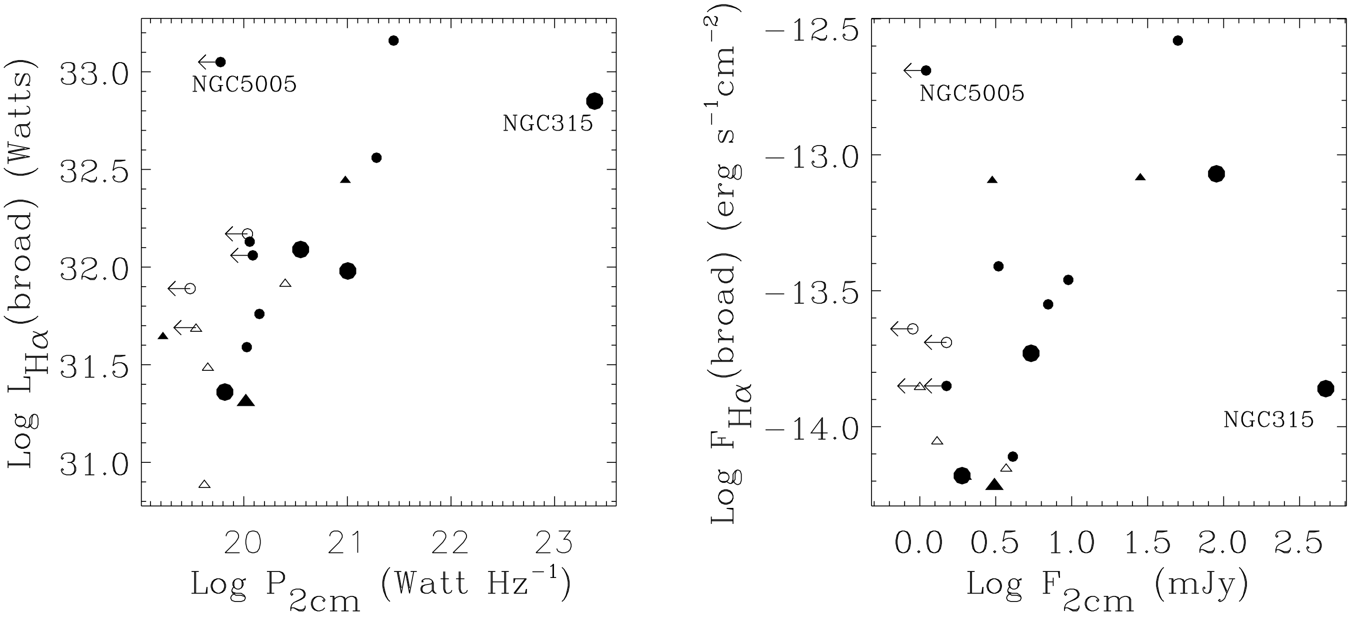

Fig. 9. (a) The luminosity of the broad component of Hα as a function of the 2 cm core (150 mas resolution) radio power for all (20) type 1.9 AGNs in the Palomar sample for which photometric broad Hα fluxes are available. LINERs are plotted as circles and Seyferts as triangles. Nuclei with definite and probable detections of broad Hα (Ho et al., 1997c) are shown with filled and open symbols, respectively. Elliptical nuclei are shown with large symbols; **(b)** same as (a) but for fluxes instead of luminosities.

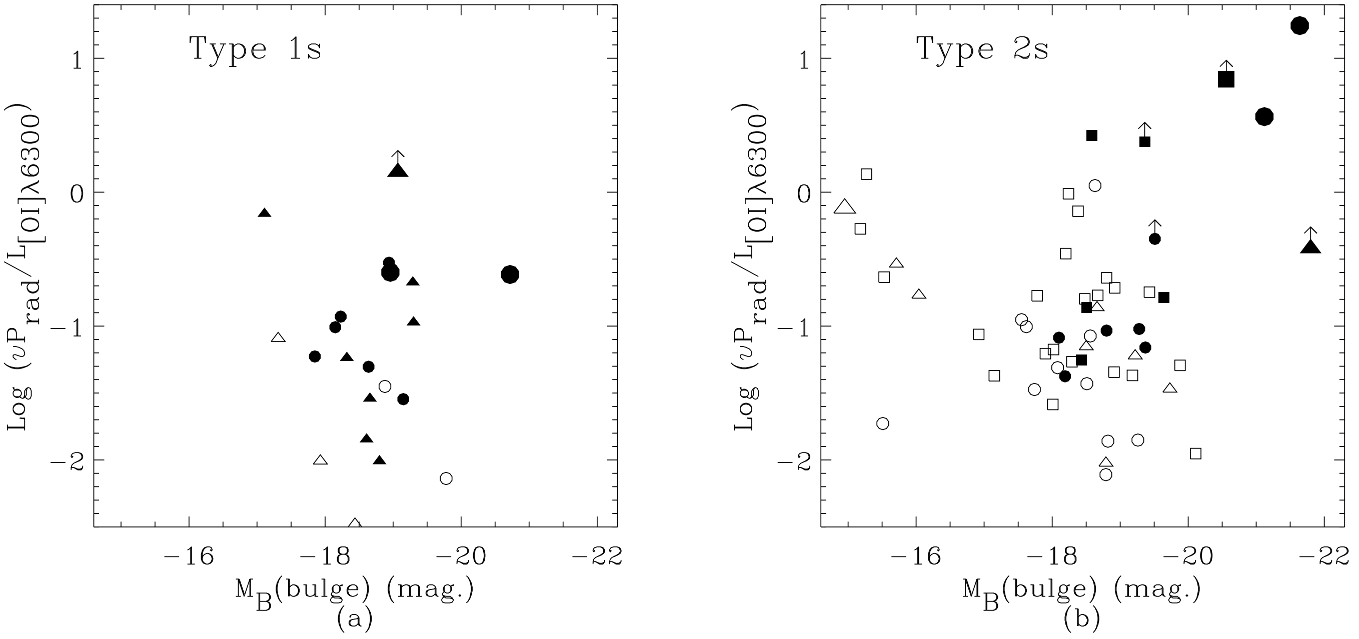

Fig. 10. The ratio of 2 cm core (150 mas resolution) radio luminosity to [O I] λ6300 luminosity as a function of galaxy bulge magnitude in the blue band for type 1 LLAGNs **(a)** and type 2 LLAGNs **(b)** in the distance-limited ($D \leq 19$ Mpc) sample. LINERs are plotted as circles, Seyferts as triangles, and transition nuclei as squares. Large symbols are used for elliptical galaxies and filled symbols are used for nuclei detected at 2 cm. Open symbols therefore represent upper limits to the true radio to emission-line luminosity ratio. Nuclei with upper limits for both radio and [O I] luminosities are not plotted.

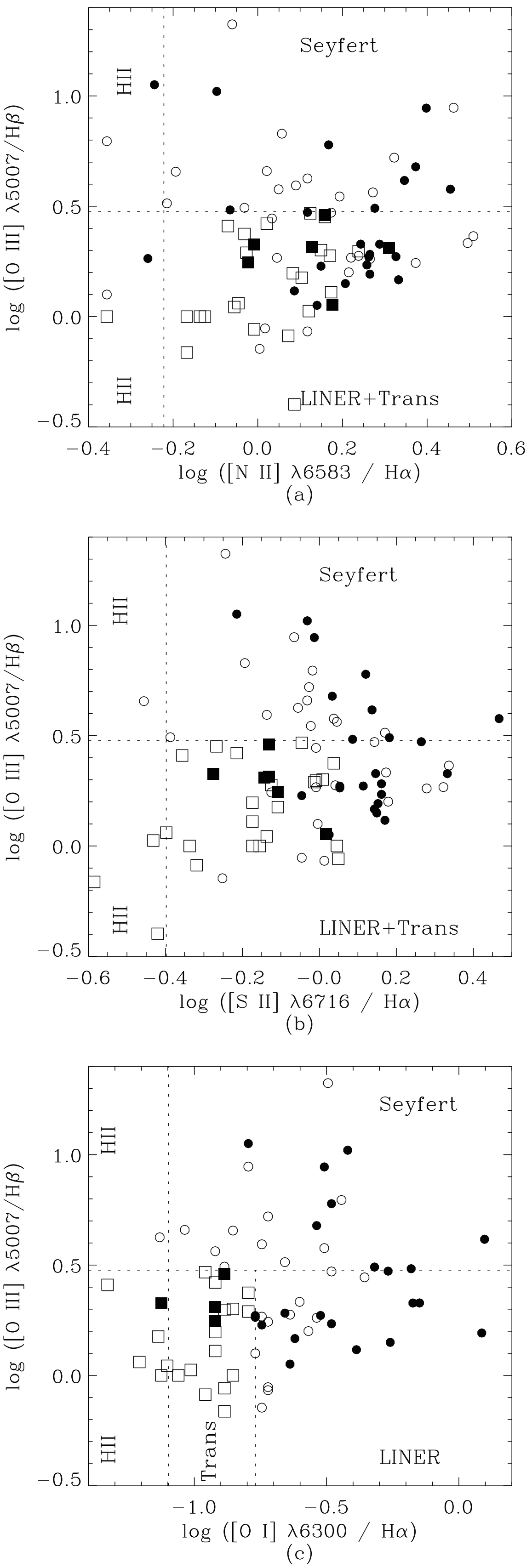

Fig. 11. Plots of standard diagnostic emission-line ratios for the D ≤ 19 Mpc LLAGNs. For clarity, nuclei with upper limits to any one of the four emission-lines in each respective panel are not plotted. Emission-line fluxes have been taken from H97a. LINERs and low-luminosity Seyferts are plotted as circles and transition nuclei are plotted as squares. Filled symbols are used for nuclei detected at 2 cm, and open symbols for nuclei not detected at 2 cm.

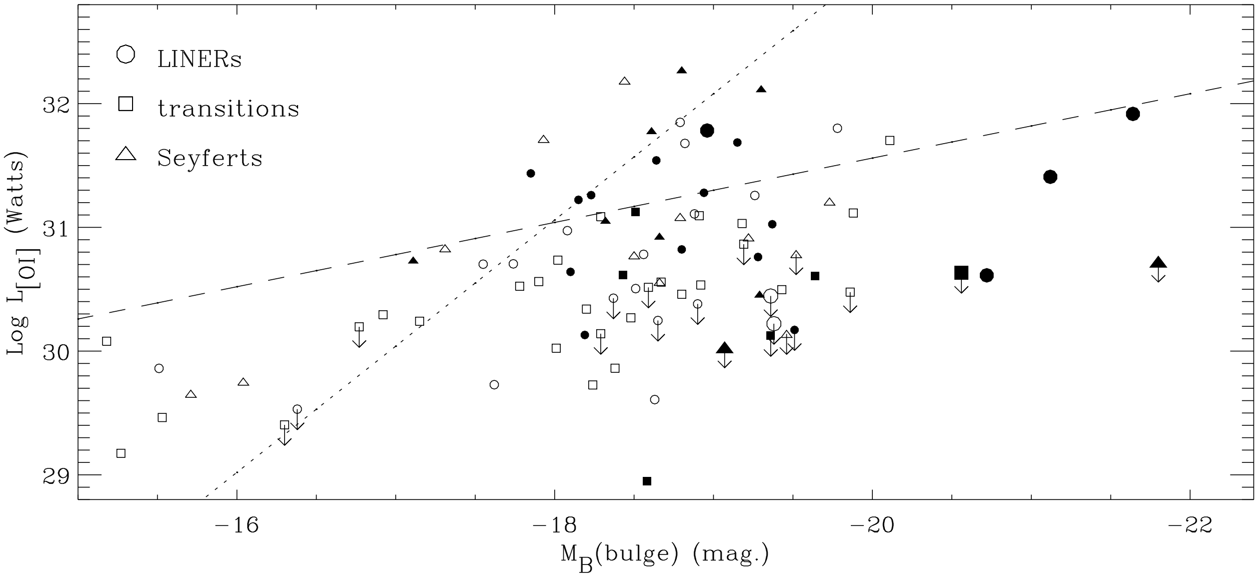

Fig. 12. The dependence of the luminosity of the [O I] λ6300 emission-line on the absolute magnitude in the blue band of the galaxy bulge for the distance-limited ($D \leq 19$ Mpc) sample. LINERs are plotted as circles, Seyferts as triangles and transition nuclei as squares. Large symbols are used for elliptical galaxies and filled symbols for radio detected nuclei. Also shown is the low-luminosity extrapolation of the linear fit to the same relationship for the luminous Seyferts in the Whittle (1992a) compilation (dotted line; see text) and an indicative low-luminosity extrapolation of the linear fit to the same relationship for FR I radio galaxies from Zirbel & Baum (1995, dashed line; see text).

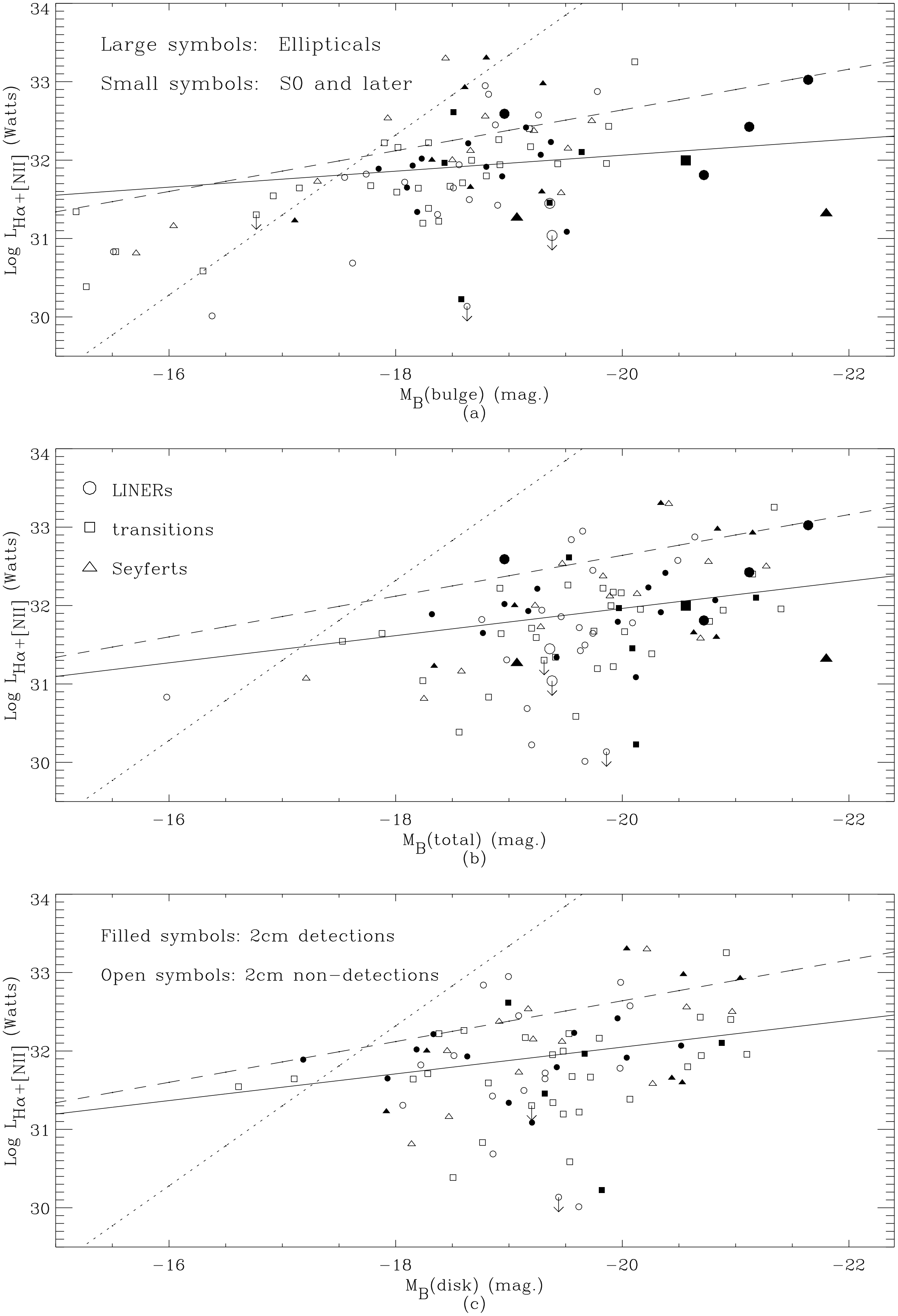

Fig. 13. The dependence of the luminosity of the Hα+[N II] λλ6548,6583 emission-lines on the absolute magnitude in the blue band of **(a)** the galaxy bulge; **(b)** the entire galaxy; and **(c)** the galaxy disk, for the distance-limited (D ≤ 19 Mpc) sample. Some of the galaxies fall beyond the left and bottom boundaries of the plots. Symbols are as in the previous figure. Linear fits to the radio-detected nuclei are shown as the solid line in each panel. Also shown in each panel is the low-luminosity extrapolation of a linear fit to the $L_{H\alpha+[N\,II]}$ vs M_B(bulge) relationship for luminous Seyferts in the Whittle (1992) compilation (dotted line; see text) and FR I radio galaxies from Zirbel & Baum (1995, dashed line).

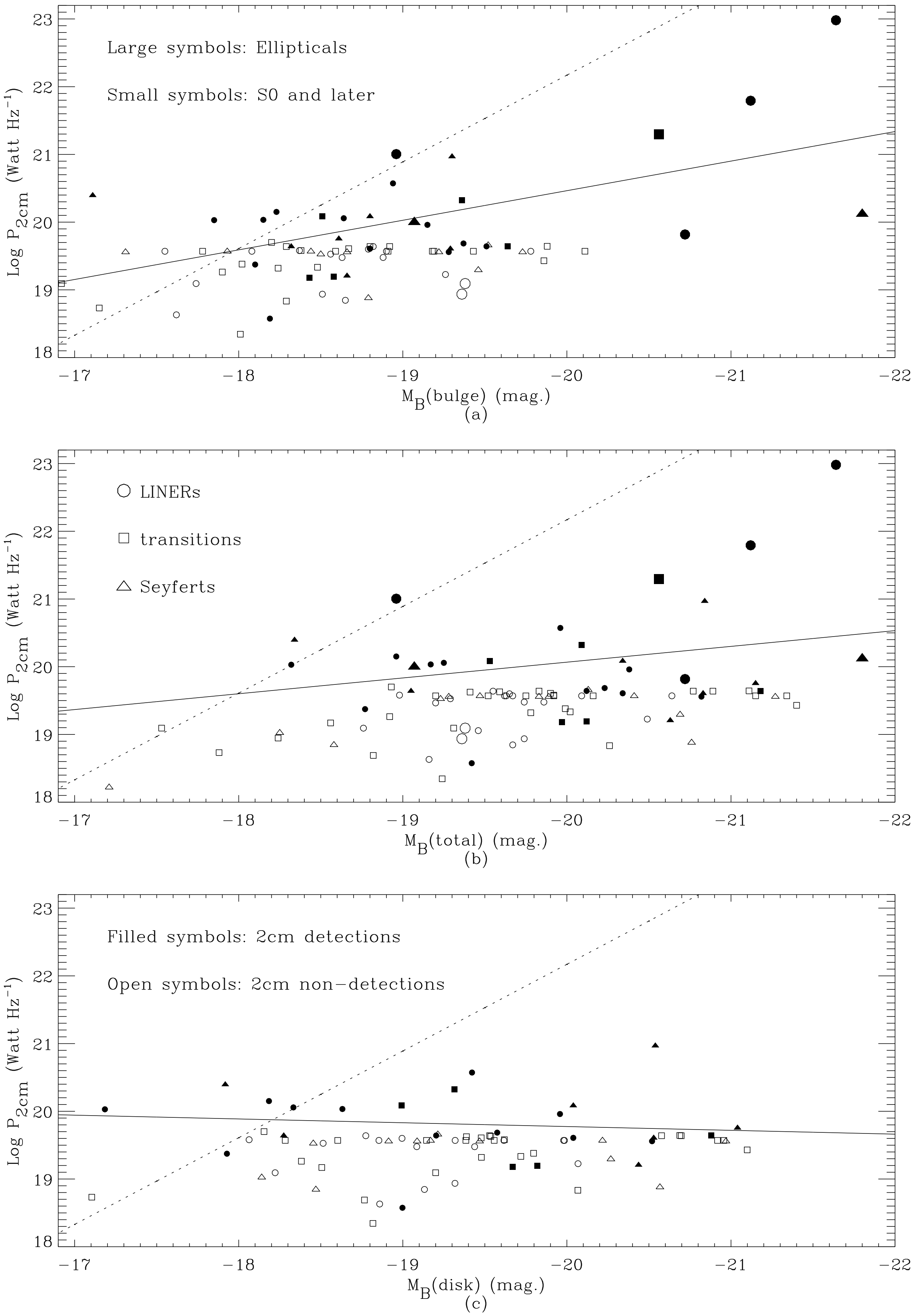

Fig. 14. As for Fig.13, but with the 2 cm core (150 mas resolution) radio power as the *y* axis. Some of the galaxies fall beyond the left and bottom boundaries of the plots. Each panel also shows the best linear fit to the radio detected nuclei (solid line), and the low-luminosity extrapolation of a linear fit to the core radio power vs bulge luminosity relationship in both luminous Seyferts and (FR I and FR II) radio galaxies (Nelson & Whittle, 1996, dotted line).

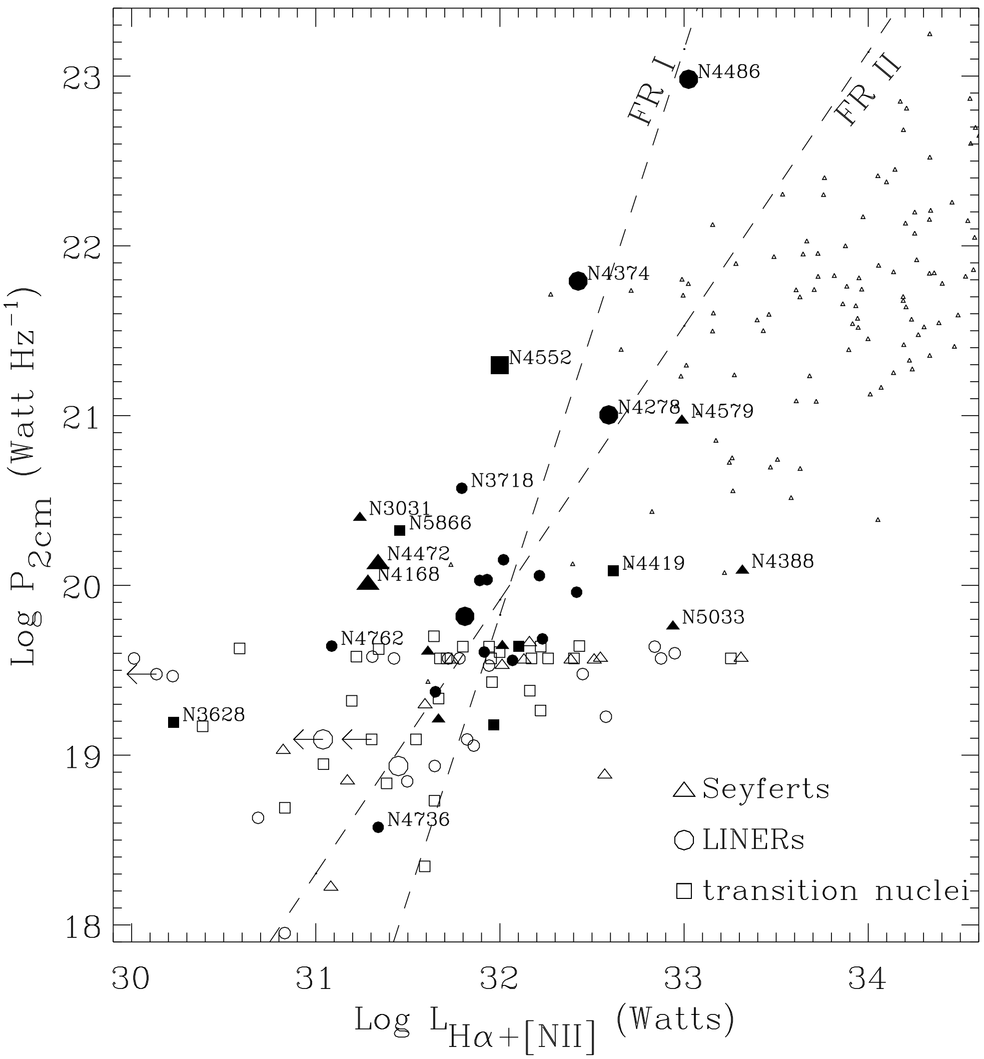

Fig. 15. A plot of 2 cm core (150 mas resolution) radio power versus nuclear Hα+[N II] $\lambda\lambda$6548,6583 luminosity for all LLAGNs in the distance-limited (D $\leq$ 19 Mpc) sample. Symbols are as used in Fig.12. "Classical" Seyfert galaxies (from Whittle 1992a) are plotted as the smallest triangles (for these the [O III] luminosity was converted to an Hα+[N II] luminosity using standard flux ratios for Seyferts, see text). Also shown are the low-luminosity extrapolations of linear fits to the same relationship for FR I and FR II radio galaxies (dashed lines; Zirbel & Baum 1995, see text).

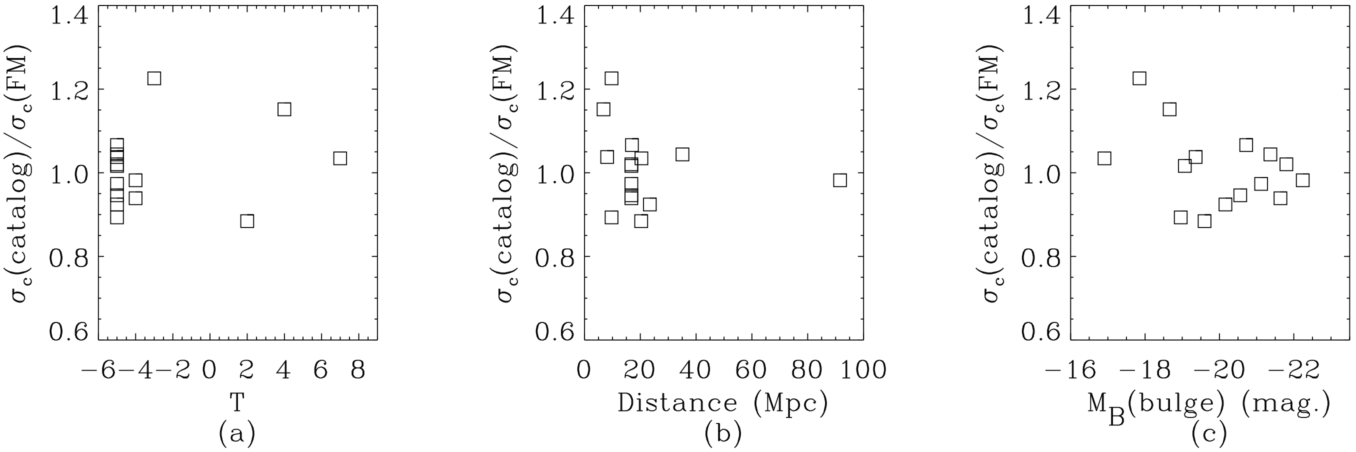

Fig. 16. The ratio of the central velocity dispersion listed in either LEDA or Hypercat to that listed in Ferrarese & Merritt (2000) and Merritt & Ferrarese (2001) is plotted against the **(a)** morphological type of the galaxy; **(b)** distance to the galaxy; and **(c)** absolute magnitude in the B band of the galaxy bulge, for galaxies in the Palomar sample. The values from these sources agree to better than ±20%.

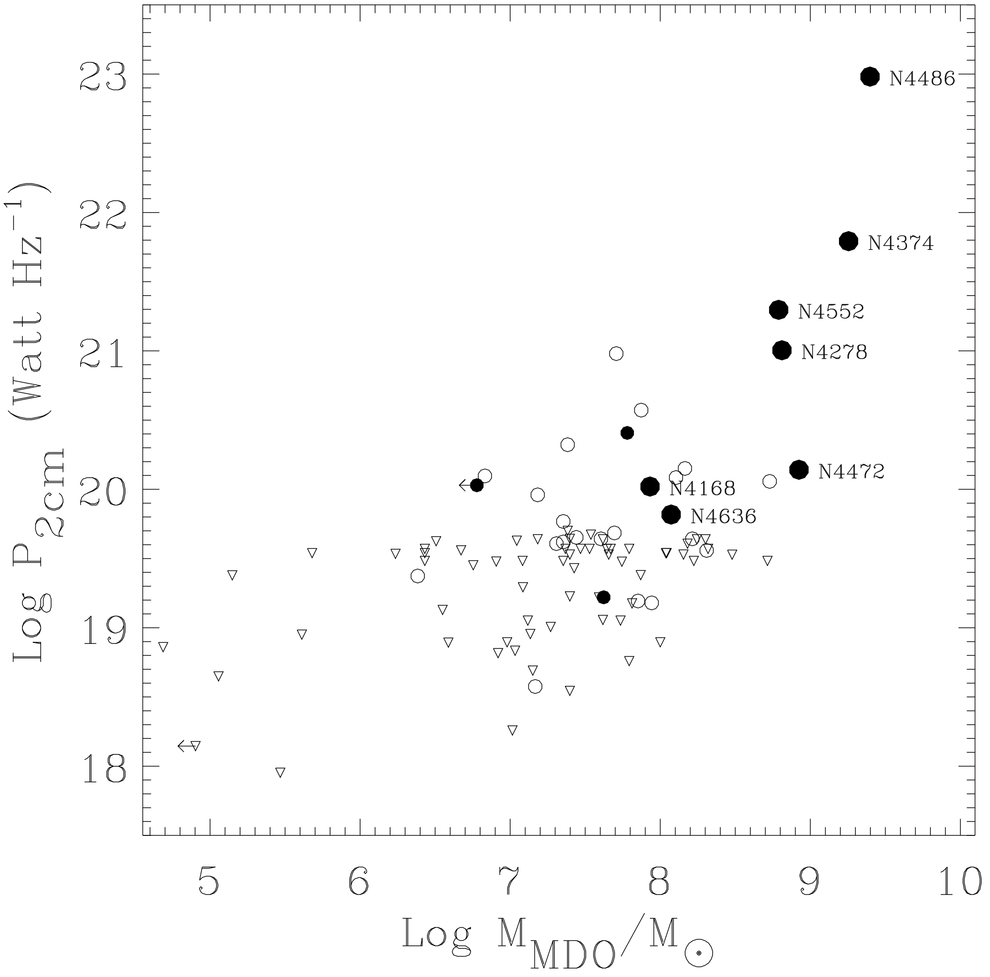

Fig. 17. Dependence of the core (150 mas resolution) 2 cm power on the mass of the supermassive black hole for LLAGNs in the distance-limited (D ≤ 19 Mpc) sample. For the radio detections, large symbols are used for ellipticals (which are labelled with their names) and filled symbols for the most reliable measurements of MDO mass (see text). All radio non-detections are shown by the downward pointing triangles. NGC 185 lies beyond the bottom left corner of the plot.

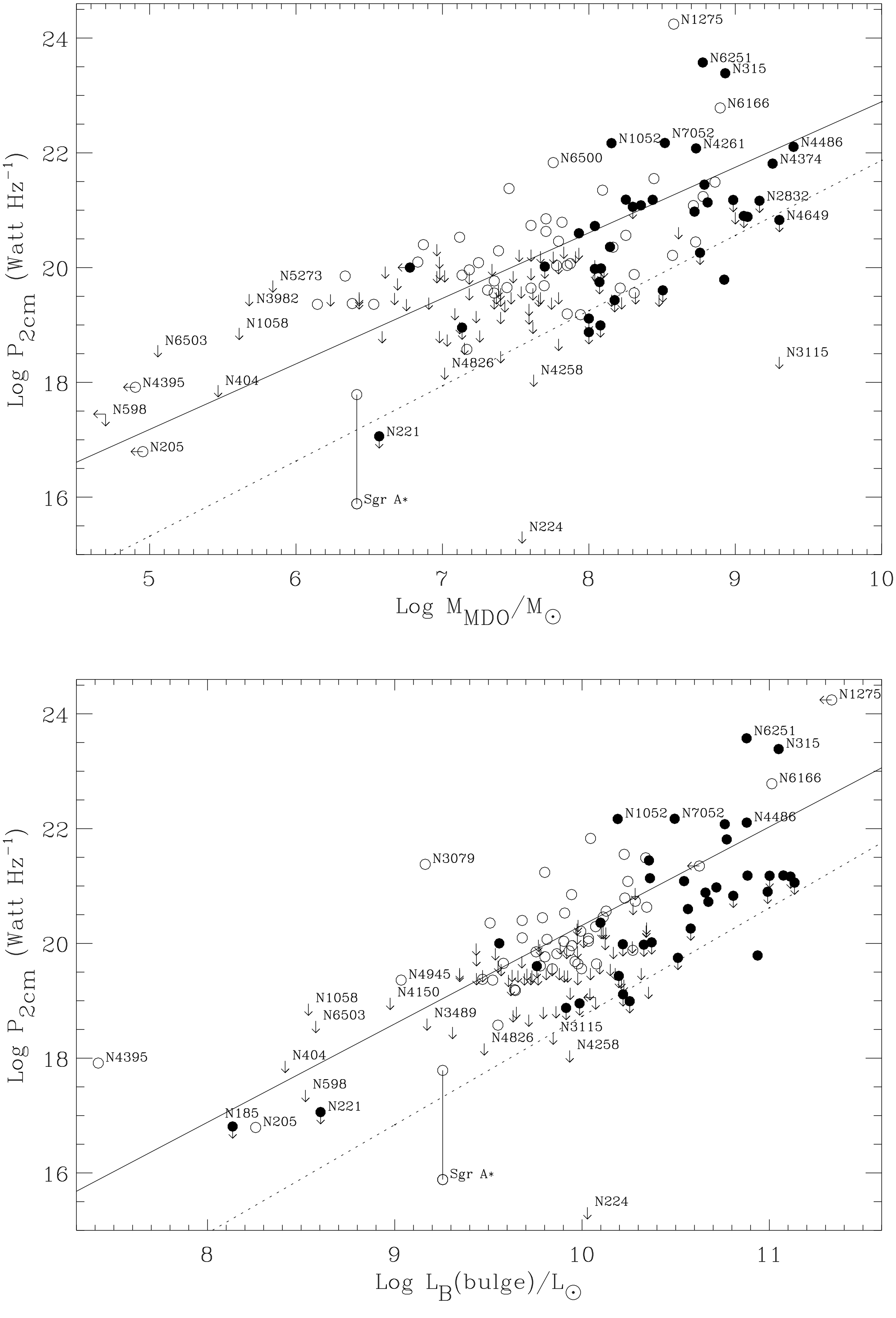

Fig. 18. Upper Panel: The dependence of the core radio power on the mass of the supermassive black hole for nearby galaxies. Only galaxies with all three of radio power, MDO estimate and L_B(bulge) are plotted. Radio flux measurements with resolution > 150 mas are plotted as upper limits. Ellipticals are plotted as filled circles and non-elliptical radio detections as open circles. For clarity the symbols for non-elliptical nuclei with radio upper limits are not plotted (only the downward pointing arrows are plotted for these). Galaxy names are provided for data points in the less crowded areas of the plots. NGC 185, with an estimated MDO mass of 6.8×10^3 $M_\odot$, lies off the left of the plot. The two values for Sgr A* correspond to radio powers within 10 mas and within $\sim 10'$. In each panel, the solid and dashed lines show the linear fits to all (66) nuclei with radio cores detected at ≤ 150 mas resolution, and all (154) nuclei plotted, respectively. The linear fits take account of the upper limits in both variables. **Lower Panel:** same as upper panel, but for bulge luminosity in the B band instead of black hole mass.

TABLE 1

THE DISTANCE- AND RADIO-FLUX-LIMITED LLAGN SAMPLE

Name (1)	Other Name (2)	Activity Type (3)	Dist. (Mpc) (4)	Ref. (5)
NGC 2787		L1.9	13.0	a
NGC 3031	M 81	S1.5	3.6	b
NGC 3718		L1.9	17.0	c
NGC 4143		L1.9	17.0	c
NGC 4168		S1.9	16.8	c
NGC 4203		L1.9	9.7	a
NGC 4258	M 106	S1.9	6.8	e
NGC 4278		L1.9	9.7	a
NGC 4374	M 84	L2	16.8	c
NGC 4472	M 49	S2	16.8	c
NGC 4486	M 87	L2	16.8	d
NGC 4552	M 89	T2	16.8	c
NGC 4565		S1.9	9.7	a
NGC 4579	M 58	S1.9	16.8	a
NGC 4772		L1.9	16.3	c
NGC 5866	M 102	T2	15.3	a

Note. — This table lists all LLAGNs from the Palomar spectroscopic sample which have D $<$ 19 Mpc and $S_{2cm}^{VLA} > 2.7$ mJy.

Note. — Columns are: **(1)** galaxy name; **(2)** other common name; **(3)** nuclear activity type as derived by H97a. 'L' represents LINER, 'S' represents Seyfert, and 'T' represents objects with transitional 'L' + 'H' spectra. '2' implies that no broad Hα is detected, '1.9' implies that broad Hα is present, but not broad Hβ, and '1.0', '1.2', or '1.5' implies that both broad Hα and broad Hβ are detected, with the specific type depending on the ratio of the flux in [O III] λ5007 to the flux in broad + narrow Hβ (Osterbrock 1981); **(4)** distance (in Mpc) to galaxy, as listed in H97a, except for NGC 3031, for which we use the distance from Freedman et al. (1994), and NGC 4258, for which we use the distance from Herrnstein et al. (1999); **(5)** source for VLBI data. a = Falcke et al. (2000a); b = Bartel et al. (1982); c = this work; d = Junor & Biretta (1995); e = Herrnstein et al. (1997).

TABLE 2
NEW 2 CM VLA OBSERVATIONS OF LOW-LUMINOSITY AGNS

Name (1)	Activity Type (2)	T (3)	R.A. (B1950) (4)	Dec. (B1950) (5)	Δ ($''$) (6)	S_{peak} (mJy/ beam) (7)	S_{tot} (mJy) (8)	Dist. (Mpc) (9)	Log P^{core}_{2cm} (W Hz^{-1}) (10)	α (11)	Com. (12)
IC 239	L2::	6.0	···	···	···	···	< 0.9	16.8	< 19.48	···	
IC 1727	T2/L2	9.0	···	···	···	···	< 0.9	8.2	< 18.86	···	
NGC 428	L2/T2:	9.0	···	···	···	···	< 0.9	14.9	< 19.38	···	
NGC 660	T2/H:	1.0	···	···	···	···	< 0.9	11.8	< 19.18	···	
NGC 1055	T2/L2::	3.0	···	···	···	···	< 1.8	12.6	< 19.53	···	
NGC 1058	S2	5.0	···	···	···	···	< 0.9	9.1	< 18.95	···	
NGC 2541	T2/H:	6.0	···	···	···	···	< 1.0	10.6	< 19.13	···	
NGC 2683	L2/S2	3.0	···	···	···	···	< 0.9	5.7	< 18.54	···	
NGC 2685	S2/T2:	–1.0	···	···	···	···	< 0.9	16.2	< 19.45	···	
NGC 2787	L1.9	–1.0	09 14 49.469	69 24 50.82	1.6	11.1	11.4	13.0	20.35	F	1
NGC 2841	L2	3.0	09 18 35.841	51 11 24.10	7.4	1.1	2.1	12.0	19.28	F	2,8,9
NGC 3031	S1.5	2.0	09 51 27.313	69 18 08.15	6.3	164.1	164.8	3.6	20.41	F	3
NGC 3368	L2	2.0	···	···	···	···	< 1.0	8.1	< 18.89	···	
NGC 3379	L2/T2::	–5.0	···	···	···	···	< 1.0	8.1	< 18.89	···	
NGC 3486	S2	5.0	···	···	···	···	< 1.0	7.4	< 18.82	···	
NGC 3489	T2/S2	–1.0	···	···	···	···	< 1.0	6.4	< 18.69	···	
NGC 3623	L2:	1.0	···	···	···	···	< 0.9	7.3	< 18.76	···	
NGC 3627	T2/S2	3.0	11 17 38.475	13 15 55.76	8.3	1.1	2.9	6.6	18.76	F	2,4,8
NGC 3628	T2	3.0	11 17 40.354	13 51 46.06	6.6	1.5	2.2	7.7	19.03	···	7,8
NGC 3675	T2	3.0	···	···	···	···	< 1.0	12.8	< 19.29	···	
NGC 3718	L1.9	1.0	11 29 49.910	53 20 38.47	2.0	10.5	10.8	17.0	20.56	F	2,9
NGC 3941	S2:	–2.0	···	···	···	···	< 1.1	18.9	< 19.67	···	
NGC 3982	S1.9	3.0	···	···	···	···	< 1.0	17.0	< 19.54	···	
NGC 4013	T2	3.0	···	···	···	···	< 1.0	17.0	< 19.54	···	
NGC 4051	S1.2	4.0	···	···	···	···	< 1.0	17.0	< 19.54	···	
NGC 4138	S1.9	–1.0	12 06 58.344	43 57 48.12	1.2	1.5	1.3	17.0	19.71	F	2,8
NGC 4143	L1.9	–2.0	12 07 04.548	42 48 44.26	1.6	9.8	10.0	17.0	20.53	F	1,9
NGC 4150	T2	–2.0	···	···	···	···	< 1.0	9.7	< 19.05	···	
NGC 4168	S1.9:	–5.0	12 09 44.270	13 28 59.62	1.0	3.0	3.1	16.8	20.01	F	2,8,10
NGC 4203	L1.9	–3.0	12 12 33.943	33 28 30.48	1.2	8.8	9.0	9.7	20.00	F	1,10
NGC 4216	T2	3.0	12 13 21.620	13 25 38.11	2.1	1.2	1.3	16.8	19.61	F	2,8,10
NGC 4258	S1.9	4.0	12 16 29.365	47 34 53.19	0.4	2.6	3.0	6.8	19.16	F	2,8,9
NGC 4278	L1.9	–5.0	12 17 36.159	29 33 29.27	1.6	83.8	87.7	9.7	20.97	F	1,10
NGC 4293	L2	0.0	12 18 40.996	18 39 34.95	5.7	0.7	1.4	17.0	19.38	S	6,8,10
NGC 4314	L2	1.0	···	···	···	···	< 1.0	9.7	< 19.05	···	
NGC 4321	T2	4.0	···	···	···	···	< 0.9	16.8	< 19.48	···	
NGC 4346	L2::	–2.0	···	···	···	···	< 1.0	17.0	< 19.54	···	
NGC 4350	T2::	–2.0	···	···	···	···	< 0.9	16.8	< 19.48	···	
NGC 4374	L2	–5.0	12 22 31.584	13 09 49.82	3.3	180.7	183.7	16.8	21.79	F	2,10
NGC 4388	S1.9	3.0	12 23 14.641	12 56 20.09	2.1	2.2	3.7	16.8	19.87	···	10
NGC 4394	L2	3.0	···	···	···	···	< 0.9	16.8	< 19.48	···	
NGC 4395	S1.8	9.0	···	···	···	···	< 0.9	3.6	< 18.14	···	
NGC 4414	T2:	5.0	···	···	···	···	< 0.9	9.7	< 19.01	···	
NGC 4419	T2	1.0	12 24 24.716	15 19 26.53	2.8	2.7	3.6	16.8	19.96	S	6,10
NGC 4438	L1.9	0.0	···	···	···	···	< 0.9	16.8	< 19.48	···	
NGC 4450	L1.9	2.0	12 25 58.284	17 21 40.94	1.5	2.0	2.7	16.8	19.83	F	2,8,10
NGC 4457	L2	0.0	···	···	···	···	< 1.0	17.4	< 19.56	···	
NGC 4459	T2:	–1.0	···	···	···	···	< 1.0	16.8	< 19.53	···	
NGC 4472	S2::	–5.0	12 27 14.183	08 16 35.99	1.9	3.7	4.1	16.8	20.10	···	
NGC 4477	S2	–2.0	···	···	···	···	< 1.0	16.8	< 19.53	···	
NGC 4486	L2	–4.0	12 28 17.568	12 40 01.74	3.1	2725.7	2835.7	16.8	22.96	F	5
NGC 4494	L2::	–5.0	···	···	···	···	< 0.8	9.7	< 18.95	···	
NGC 4501	S2	3.0	···	···	···	···	< 1.1	16.8	< 19.57	···	
NGC 4548	L2	3.0	12 32 55.275	14 46 17.67	2.5	1.4	1.6	16.8	19.67	F	1,8,9
NGC 4552	T2:	–5.0	12 33 08.293	12 49 53.58	2.7	58.1	58.6	16.8	21.29	F	2

TABLE 2—*Continued*

Name (1)	Activity Type (2)	T (3)	R.A. (B1950) (4)	Dec. (B1950) (5)	Δ ($''$) (6)	$S_{\rm peak}$ (mJy/ beam) (7)	$S_{\rm tot}$ (mJy) (8)	Dist. (Mpc) (9)	Log $P^{\rm core}_{\rm 2cm}$ (W Hz^{-1}) (10)	α (11)	Com. (12)
NGC 4565	S1.9	3.0	12 33 52.017	26 15 45.89	4.4	3.1	3.1	9.7	19.54	F	1,8,11
NGC 4579	S1.9/L1.9	3.0	12 35 11.999	12 05 34.85	3.1	20.8	20.6	16.8	20.85	F	1
NGC 4596	L2::	–1.0	···	···	···	···	< 1.1	16.8	< 19.57	···	
NGC 4636	L1.9	–5.0	12 40 16.661	02 57 41.59	2.6	1.6	1.8	17.0	19.74	···	8
NGC 4698	S2	2.0	···	···	···	···	< 1.0	16.8	< 19.53	···	
NGC 4713	T2	7.0	···	···	···	···	< 1.1	17.9	< 19.63	···	
NGC 4725	S2:	2.0	···	···	···	···	< 0.9	12.4	< 19.22	···	
NGC 4736	L2	2.0	12 48 31.915	41 23 31.35	6.3	1.9	1.7	4.3	18.62	F	2,8
NGC 4762	L2:	–2.0	12 50 25.139	11 30 03.27	2.8	0.9	1.3	16.8	19.48	F	2,8
NGC 4772	L1.9	1.0	12 50 56.003	02 26 22.36	2.5	3.3	3.4	16.3	20.02	F	2,8
NGC 4826	T2	2.0	···	···	···	···	< 0.9	4.1	< 18.26	···	
NGC 5194	S2	4.0	···	···	···	···	< 1.1	7.7	< 18.89	···	
NGC 5195	L2:	10.0	···	···	···	···	< 1.1	9.3	< 19.06	···	
NGC 5879	T2/L2	4.0	···	···	···	···	< 1.1	16.8	< 19.57	···	
NGC 6503	T2/S2:	6.0	···	···	···	···	< 1.0	6.1	< 18.65	···	
NGC 7177	T2	3.0	···	···	···	···	< 1.1	18.2	< 19.64	···	
NGC 7331	T2	3.0	···	···	···	···	< 1.1	14.3	< 19.43	···	

Note. — Columns are: **(1)** galaxy name; **(2)** nuclear activity type as given by H97a. 'L' represents LINER, 'S' represents Seyfert, 'H' represents an H II region type spectrum, and 'T' represents objects with transitional 'L' + 'H' spectra. '2' implies that no broad Hα is detected, '1.9' implies that broad Hα is present, but not broad Hβ, and '1.0' or '1.5' implies that both broad Hα and broad Hβ are detected, with the specific type depending on the ratio of the flux in [O III] λ5007 to the flux in broad + narrow Hβ (Osterbrock 1981). The ':' and '::' symbols represent uncertain, and highly uncertain, classifications, respectively; **(3)** Hubble morphological parameter T as listed in H97a; **(4)** and **(5)** 2 cm radio position; **(6)** offset, in arcsec, between the 2 cm radio position and the position of the galaxy optical nucleus listed in Cotton et al. (1999); **(7)** and **(8)** peak flux-density and total flux, obtained by fitting a single Gaussian (with peak flux-density, major and minor axes as free parameters) to the nuclear radio source in our maps. Fluxes were derived from maps with resolution $\sim$ 150 mas for all radio detected sources (see Sect. 4.1). For most sources, the 1σ error in the flux determination comes from a 2.5% flux-bootstrapping error and the 0.2 mJy r.m.s. noise in the final maps. Additional errors in the flux determination, if present, are listed in the comments column; **(9)** distance to galaxy, as listed in H97a, except for NGC 3031 for which we use the distance from Freedman et al. (1994); **(10)** the logarithm of the core radio power (derived from the *peak* radio flux-density); **(11)** indication of whether the radio spectrum of the 2 cm detected core is **S**teep ($\alpha <$ –0.3; $S_\nu \propto \nu^\alpha$), or **F**lat ($\alpha \geq$ –0.3); **(12)** comments as listed below.

Note. — Comments: **1**: column 11 taken from Nagar et al. (2000); **2**: column 11 derived from comparison with FIRST; **3**: column 11 derived from comprison with NVSS; **4**: column 11 derived from comparison with Laurent-Muehleisen et al. (1997); **5**: column 11 derived from Nagar et al. (2001); **6**: column 11 derived from VLA archive data (see Sect. 4.1); **7**: the total 2 cm flux we measured, including the extended starburst region, is 28 mJy; **8**: accurate self-calibration was not possible, therefore the measured flux may be lower than the true flux due to decorrelation losses; **9**: additional $\sim$1.5% flux error due to elevation effects. **10**: additional $\sim$2.5% flux error due to elevation effects. **11**: additional $\sim$4% flux error due to elevation effects.

TABLE 3
NEW OBSERVATIONS OF LLAGN WITH THE VLBA

Name (1)	Activity Type (2)	R.A. (J2000) (3)	DEC. (J2000) (4)	Peak Flux (mJy/beam) (5)	Total Flux (mJy) (6)	Beam (mas) (7)	Beam (pc) (8)	Beam P.A. (9)	Log T_B (K) (10)	Com. (11)
NGC 2655	S2	···	···	<0.76	···	4.8×4.3	0.57×0.51	45.0	<6.4	a,g
NGC 3147	S2	10 16 53.6509	73 24 02.695	6.1	8.1	1.6×1.3	0.32×0.25	26.8	>8.3	a
NGC 3718	L1.9	11 32 34.8530	53 04 04.518	3.4	5.3	2.2×1.7	0.18×0.14	–54.3	>7.8	b
NGC 4143	L1.9	12 09 36.0679	42 32 03.036	8.1	8.7	2.3×1.2	0.19×0.10	–41.2	>8.3	
NGC 4168	S1.9	12 12 17.2685	13 12 18.701	2.5	2.4	3.2×1.6	0.26×0.13	10.3	>7.6	b
NGC 4374 (Core)	L2	12 25 03.7433	12 53 13.142	160.0	160.0	2.7×1.4	0.22×0.11	6.6	≥9.5	
NGC 4374 (North)		···	···	11.9	16.6				···	c
NGC 4374 (North2)		···	···	2.4	2.4				···	c,d
NGC 4374 (South)		···	···	7.0	7.0				···	c
NGC 4472	S2	12 29 46.7619	08 00 01.713	2.2	2.3	3.4×1.5	0.28×0.12	5.2	>7.5	b
NGC 4552 (Core)	T2	12 35 39.8073	12 33 22.829	99.5	99.5	2.9×1.2	0.23×0.10	2.4	≥9.3	
NGC 4552 (East1)		···	···	7.9	7.9				···	c
NGC 4552 (East2)		···	···	5.3	14.6				···	c,e
NGC 4552 (West)		···	···	9.8	17.0				···	c
NGC 4772	L1.9	12 53 29.1613	02 10 06.157	1.8	1.3	5.0×4.0	0.39×0.32	0	>6.8	b,f

Note. — Columns are: (1) galaxy name; (2) activity type as derived by H97a and explained in the footnotes to Table 1; (3) and (4) nuclear radio position. Positions were determined by first fitting a Gaussian to the central component in the non-self-calibrated VLBA maps, and then correcting the measured positions to reflect the more accurate phase calibrator positions now available (see Sect. 4.3); (5) and (6) peak flux-density and total flux, measured, unless noted otherwise, by fitting a Gaussian to the final map; (7) the major and minor axes of the synthesized beam in milliarcsec (mas); (8) the major and minor axes of the synthesized beam in parsec using the distance listed in H97a; (9) the position angle (P.A.) of the beam in degrees, measured N through E; (10) logarithm of the brightness temperature in Kelvin of the radio core derived using the formula listed in Falcke et al. (2000a). Since most of the sources are unresolved, the values from the formula are usually lower limits to the true brightness temperature; (11) comments as listed below.

Note. — Comments: (a) not in the sample listed in Table 1; (b) peak flux-density (from non-self-calibrated map) multiplied by 1.3 to account for decorrelation losses (see Sect. 3.2); (c) from a single Gaussian fit; (d) northernmost component in Fig. 1a; (e) easternmost component in Fig. 1b; (f) all data from the longest baselines (to antennas on Mauna Kea and Saint Croix), were deleted because of large phase wraps; (g) the peak flux-density listed is a 10σ upper limit, from a naturally weighted map, obtained after deleting all data from the antennas at Mauna Kea and Saint Croix.

TABLE 4

RESULTS OF BIVARIATE STATISTICAL COMPARISONS FOR THE DISTANCE-LIMITED ($D \leq 19$ MPC) LLAGN SAMPLE

Sub-sample (1)	Variable A (2)	Variable B (3)	Cox (4)	Kendall τ (5)	Spearman ρ (6)
All (31) LLAGNs with 2 cm radio cores in the distance-limited ($D \leq 19$ Mpc) sample					
All nuclei	M_B(bulge)	P_{2cm}	98.5	92.5	92.5
	M_B(total)	P_{2cm}	71.0	31.0	21.0
	M_B(bulge)	$L_{H\alpha+[N II]}$	73.0	68.0	66.0
	M_B(total)	$L_{H\alpha+[N II]}$	92.7	88.0	89.0
	$L_{H\alpha+[N II]}$	P_{2cm}	98.8	97.7	97.0
	$L_{[O I]}$	P_{2cm}	99.99	99.32	98.4
	FWHM([N II])	$L_{[N II]}$	99.06	99.47	99.51
	FWHM([N II])	P_{2cm}	99.99	99.99	99.97
	$L_{[N II]}$	P_{2cm}	99.15	98.5	97.6
	M_{MDO}	P_{2cm}	99.75	99.28	99.10
	P_{2cm}	FWHM([N II])/ΔV^c_{rot}	99.97	99.94	99.91
S0 and later only (24 galaxies)	$L_{[O I]}$	P_{2cm}	99.94	99.64	99.30
	$L_{H\alpha+[N II]}$	P_{2cm}	88.81	93.72	91.39
	P_{2cm}	FWHM([N II])/ΔV^c_{rot}	98.3	99.20	99.29
As above, plus all LINERs and Seyferts not detected at 2 cm in the distance-limited ($D \leq 19$ Mpc) sample					
All nuclei	M_B(bulge)	P_{2cm}	99.88	99.82	99.87
	M_B(total)	P_{2cm}	99.54	94.9	98.2
	$L_{H\alpha+[N II]}$	P_{2cm}	···	99.16	99.49
	$L_{[O I]}$	P_{2cm}	···	99.97	99.97
All LLAGNs not detected at 2 cm in the distance-limited ($D \leq 19$ Mpc) sample					
All nuclei	M_B(bulge)	$L_{H\alpha+[N II]}$	99.99	99.99	99.99
	M_B(total)	$L_{H\alpha+[N II]}$	99.87	99.99	99.99
All LLAGNs in the distance-limited ($D \leq 19$ Mpc) sample					
All nuclei	M_B(bulge)	$L_{H\alpha+[N II]}$	99.98	99.99	99.99
	M_B(disk)	$L_{H\alpha+[N II]}$	90.1	95.8	95.8
	M_B(total)	$L_{H\alpha+[N II]}$	99.92	99.91	99.90
	$L_{H\alpha+[N II]}$	P_{2cm}	···	99.55	99.90
	$L_{[O I]}$	P_{2cm}	···	99.99	99.99
	M_{MDO}	P_{2cm}	···	99.99	99.99
Ellipticals only	M_B(bulge)	$L_{H\alpha+[N II]}$	94.7	79.0	70.0
S0 and later only	M_B(bulge)	$L_{H\alpha+[N II]}$	99.8	99.99	99.99
LINERs only	ΔV^c_{rot}	FWHM([NII])	99.69	99.89	99.90
Radio-detected LINERs only	ΔV^c_{rot}	FWHM([NII])	81.5	95.7	95.8
Transition nuclei only	ΔV^c_{rot}	FWHM([NII])	97.0	98.6	98.5

Note. — Columns are: (1) the nuclei considered; (2) the independent variable; (3) the dependent variable; (4) result of the Cox proportional hazard test; (5) result of the generalized Kendall τ test; (6) result of the Spearman ρ test; the values listed in columns (4), (5) and (6) are the percentage 'significance' of the correlation. The probability of getting the correlation inferred from the data when no actual correlation exists between the two variables is 100% minus the quoted value of the significance i.e. high percentages imply a low chance that the observed correlation is spurious. For easier reading, probabilities less than 99% are listed to only one decimal place. Asurv statistical tests take into account upper or lower limits in the data. The Cox proportional test allows upper limits in only one of the variables; this test could not be applied in some of the cases above.

TABLE 5

RESULTS OF BIVARIATE STATISTICAL COMPARISONS FOR THE MDO SAMPLE

Variable A (1)	Variable B (2)	Cox (3)	Kendall τ (4)	Spearman ρ (5)
All (154) galaxies				
M_{MDO}	P_{2cm}	99.99	99.99	99.99
L_B(bulge)	P_{2cm}	99.99	99.99	99.99
Ellipticals only (37 galaxies)				
M_{MDO}	P_{2cm}	98.5	99.48	99.81
L_B(bulge)	P_{2cm}	98.4	98.5	99.64
S0 and later only (117 galaxies)				
M_{MDO}	P_{2cm}	99.98	99.99	99.99
L_B(bulge)	P_{2cm}	99.78	99.99	99.98
Radio detections only (66 galaxies)				
M_{MDO}	P_{2cm}	99.99	99.99	99.99
L_B(bulge)	P_{2cm}	99.99	99.99	99.99

Note. — Columns 1 to 5 are equivalent to columns 2 to 6 of Table 4 and are explained in the footnote to Table 4.